

Run-and-tumble particles with 1D Coulomb interaction: the active jellium model and the non-reciprocal self-gravitating gas

Léo Touzo¹ and Pierre Le Doussal¹

¹*Laboratoire de Physique de l'Ecole Normale Supérieure,
CNRS, ENS and PSL Université, Sorbonne Université,
Université Paris Cité, 24 rue Lhomond, 75005 Paris, France*

(Dated: February 14, 2025)

Recently we studied N run-and-tumble particles in one dimension – which switch with rate γ between driving velocities $\pm v_0$ – interacting via the long range 1D Coulomb potential (also called rank interaction), both in the attractive and in the repulsive case, with and without a confining potential. We extend this study in two directions. First we consider the same system, but inside a harmonic confining potential, which we call "active jellium". We obtain a parametric representation of the particle density in the stationary state at large N , which we analyze in detail. Contrary to the linear potential, there is always a steady-state where the density has a bounded support. However, we find that the model still exhibits transitions between phases with different behaviors of the density at the edges, ranging from a continuous decay to a jump, or even a shock (i.e. a cluster of particles, which manifests as a delta peak in the density). Notably, the interactions forbid a divergent density at the edges, which may occur in the non-interacting case. In the second part, we consider a non-reciprocal version of the rank interaction: the $+$ particles (of velocity $+v_0$) are attracted towards the $-$ particles (of velocity $-v_0$) with a constant force b/N , while the $-$ particles are repelled by the $+$ particles with a force of same amplitude. In order for a stationary state to exist we add a linear confining potential. We derive an explicit expression for the stationary density at large N , which exhibits an explicit breaking of the mirror symmetry with respect to $x = 0$. This again shows the existence of several phases, which differ by the presence or absence of a shock at $x = 0$, with one phase even exhibiting a vanishing density on the whole region $x > 0$. Our analytical results are complemented by numerical simulations for finite N .

CONTENTS

I. Introduction	2
II. Main results	4
A. Rank interaction with a harmonic external potential	4
B. Non reciprocal rank interaction	8
C. Outline of the paper	11
III. Active rank diffusions in a harmonic trap	11
A. General equations for the rank fields	11
B. A parametric representation for the stationary state in a general confining potential	12
C. A general class of solutions for the harmonic potential	12
D. Non-interacting case $\kappa = 0$	14
E. Special case $a = 1/2$, i.e. $\mu = 2\gamma$	15
1. Solution in the absence of shocks and repulsive case $\kappa > 0$	16
2. Attractive case $\kappa = -\bar{\kappa} < 0$	18
F. General case (arbitrary a)	20
1. Presence of shocks	20
2. Sign of C and the special line $\frac{\mu}{\gamma} = 1 + \frac{\kappa}{v_0}$	21
3. Edge behaviour (in the absence of shocks)	22
G. Phase diagram	25
H. Limit of small γ and fixed points	25
IV. Non-reciprocal active rank diffusions in a linear potential	27
A. Equation for the rank fields for a general non-reciprocal interaction	27
B. A simple example of non-reciprocal interaction	28
1. Phase I: Absence of shock	31
2. Phase II: Shock at $x = 0$ and no particles for $x > 0$	32
3. Phase III: Shock at $x = 0$	34
V. Conclusion	35
A. "Vision cone" model	36
References	36

I. INTRODUCTION

Active particles are systems which transform external energy into directed motion, leading to interesting out-of-equilibrium dynamics. The simplest model of an active, self propelled particle is the run-and-tumble particle (RTP). It is driven by telegraphic noise [1–5], and mimics the motion of E. Coli bacteria [6, 7]. It also arises in quasi-1D channels with staggered flows [8, 9]. Even a single RTP, when submitted to an external trapping potential, reaches a non-trivial and non-Boltzmann stationary state, where activity remains relevant at large times [1, 10–15]. Due to the simplicity of the RTP models, analytical solutions are sometimes possible. There is thus much to gain by studying them, as a starting point to elaborate more precise and detailed theories for the many complex phenomena exhibited by active matter, see e.g. [6, 7, 16–20]. To this aim it is important to investigate what happens to these stationary states in the presence of interactions between the RTP's.

Interacting active particles exhibit remarkable collective effects, such as motility-induced phase separation, clustering and jamming even for repulsive interactions and in the absence of alignment [7, 16, 18, 21–30]. To describe the effects of interactions beyond numerical simulations, hydrodynamic approaches and perturbative exact results have been developed [7, 27, 31–33]. However, there are at present very few exact results, even

in one dimension, beyond the case of two interacting RTP's on the line [25, 26, 34–39], or for harmonic chains [40–43]. Recently, exact solutions were also obtained for some specific many-particle models on a 1D lattice with contact interactions [44–47]. In the continuum, an active version of the Dyson Brownian motion was introduced, where RTP's interact in 1D via a long range, logarithmic potential, for which some analytical predictions were possible [48].

Another type of long range interaction amenable to some exact results is the Coulomb potential in 1D, which is linear in the distance. It is also called the rank interaction since the Coulomb force (either attractive or repulsive) acting on each particle is proportional to its rank, i.e., the number of particles in front of it, minus the number of particles behind. It has been much studied in the case of Brownian particles, in mathematics [49, 50], in finance [51] and in physics. In physics, most studies have addressed the equilibrium steady state, known as the self-gravitating 1D gas in the attractive case [52–54], and as the Jellium model in the repulsive case in presence of a harmonic confining potential [55–65]. The non-equilibrium dynamics of this model was studied more recently in [66, 67] using connections with the Lieb-Liniger delta Bose gas model and the Burgers equation.

Recently we have considered an active generalization of this model, consisting in N RTP's in 1D mutually interacting via the linear Coulomb potential [68]. It was solved previously for $N = 2$ leading to a two particle stationary bound state in the attractive case [34]. In the limit $N \rightarrow +\infty$, we showed that the evolution of the density fields is described by two coupled Burger's type equations. In the attractive case, and in the absence of external potential, these equations admit an exact stationary solution, which describes a N -particle bound state. This bound state was found to exhibit transitions between (i) a phase where the density is smooth with infinite support, (ii) a phase where the density has finite support and exhibits "shocks", i.e. clusters of particles, at the edges, and (iii) a fully clustered phase. The formation of these clusters is possible because of the non-analytic behavior of the Coulomb potential at the origin. Adding a linear external potential, both in the attractive and the repulsive case, makes the phase diagram even richer: additional partially expanding phases appear, with or without shocks.

The aim of the present paper is two-fold. In the first part, we want to extend the result of this previous work to a more natural confining potential, namely the harmonic well, leading to an "active jellium model" (which we will consider both for repulsive and attractive interactions). Given the form of the interaction, the linear potential was easier to treat analytically. The harmonic potential is more difficult to analyze. We are still able to obtain a parametric representation of the stationary density, but which is less explicit than for the linear potential. Nevertheless we are able to extract a lot of information about the stationary state, such as the phase diagram, the size of the support, the behavior of the densities near the edges, as well as the presence or not of shocks, i.e. of clusters of particles. These predictions are tested through numerical simulations.

The second part addresses the case of non-reciprocal interactions between right moving (+ particles) and left moving particles (– particles). As an example we consider the case where the + particles are attracted to the – particles, while the – particles are repelled by the + particles (and two particles with the same sign do not interact together), which we call the "non-reciprocal active self-gravitating gas". Indeed there has been much recent interest in collective effects in systems with non-reciprocal interactions with remarkable phenomena such as pattern formation, synchronization and flocking, see e.g. [69]. Non-reciprocal interactions are relevant in the context of animal behavior [70], and have been studied experimentally in bacteria [71], but can also be observed at smaller scales [72]. Recently, models of active particles with various form of non-reciprocal interactions (from simple forces to alignment interactions and quorum sensing) have been studied either numerically or through the analysis of general field theories or hydrodynamic equations obtained by coarse-graining of a microscopic model [73–88]. These systems often exhibit very rich phase diagrams with phase separations, pattern formation and oscillating phases. These models often involve two or more distinct "species" of active particles between which the non-reciprocal interactions take place [73–80]. There are however cases where the non-reciprocal interaction instead depends on the current "state" of the particle (such as its orientation, + or – in the present model), in particular in models with vision cones where particles only interact with the particles inside a certain angle with respect to their orientation [81–88]. The effect of such interactions on flocking in particular has attracted a lot of attention. The model considered here is somewhat closer to the second category, since the non-reciprocal interaction depends on the state of the particle, which changes with time. This choice is motivated by the objective to keep the model as analytically tractable as possible. It allows us to obtain an exact analytical solution for the stationary state and to obtain

the phase diagram. We find that here the non-reciprocity leads to a breaking of the spatial parity symmetry. Finally, as discussed above, a peculiar feature of the Coulomb interaction in one dimension is the appearance of shocks, both in the passive and active case. It is thus an interesting question to investigate how some amount of non-reciprocity in the $+/-$ interaction will affect the structure of the shocks. We find that in presence of a confining linear potential the non-reciprocity produces phases with shocks which were absent in the reciprocal case.

We have also considered a different model with non-reciprocal interactions, more directly inspired from the notion of vision cone, where the particles only receive a force (still independent of the distance) from the particles "in front" of them (i.e. on the right for $+$ particles and on the left for $-$ particles). It turns out that this model can be mapped to the reciprocal active rank diffusion model studied in [68] and in the first half of this paper, so that the non-reciprocity does not play any particular role in this case. The details are given in Appendix A.

II. MAIN RESULTS

A. Rank interaction with a harmonic external potential

We consider the active rank diffusion model introduced in [68]

$$\frac{dx_i}{dt} = \frac{\kappa}{N} \sum_{j=1}^N \text{sgn}(x_i - x_j) - V'(x_i) + v_0 \sigma_i(t) + \sqrt{2T} \xi_i(t). \quad (1)$$

This model was studied in [68] for $V(x) = 0$ and for $V(x) = a|x|$ with $a > 0$, in the absence of thermal noise ($T = 0$), where a complete analytical solution was obtained for the stationary state when it exists, or for the large time scaling form otherwise, both in the repulsive case $\kappa > 0$ and in the attractive case $\kappa = -\bar{\kappa} < 0$. For sufficiently strong attraction all the particles are grouped in a single cluster. For weaker attraction they either form a phase with a smooth density, which extends to infinity, or a phase where the density has a finite support and with "shocks" at the edges, i.e. clusters of same sign particles forming delta peaks in the density. For sufficiently repulsive interactions, $\kappa > a$, a finite fraction of the particles escape to infinity.

Here we will consider the case of a harmonic external potential

$$V(x) = \frac{\mu}{2} x^2 \quad (2)$$

(again at $T = 0$). The model (1) then has two dimensionless parameters, namely

$$\frac{\mu}{\gamma} \quad \text{and} \quad \frac{\kappa}{v_0}. \quad (3)$$

Although we cannot obtain a fully explicit solution in all cases, some analytical progress can still be made. Let us recall that for $v_0 = 0$, i.e. in the passive case, and $\kappa > 0$, the equilibrium density at $T = 0$ for sufficiently confining convex potentials is given by $\rho_{eq}(x) = V''(x)/(2\kappa)$ (within a finite support), while for $T > 0$ and for a harmonic potential it is given by Eqs. (27)-(28) in [66].

Here we study the time dependent density fields $\rho_\sigma(x, t)$ with $\sigma = \pm 1$ and their even and odd components ρ_s and ρ_d , defined as

$$\rho_\sigma(x, t) = \frac{1}{N} \sum_i \delta(x_i(t) - x) \delta_{\sigma_i(t), \sigma}, \quad (4)$$

$$\rho_{s/d}(x, t) = \rho_+(x, t) \pm \rho_-(x, t). \quad (5)$$

Since the potential is confining and the amplitude of the noise and interaction strength are finite, these densities will always have a finite support $[-x_e, x_e]$.

Let us first recall the case without interactions $\kappa = 0$. In that case it is known that the stationary densities take the form [12]

$$\rho_s(x) = \frac{2}{4^{\gamma/\mu} B(\frac{\gamma}{\mu}, \frac{\gamma}{\mu})} \frac{\mu}{v_0} \left(1 - \left(\frac{\mu x}{v_0} \right)^2 \right)^{\frac{\gamma}{\mu} - 1}, \quad \rho_d(x) = \frac{\mu x}{v_0} \rho_s(x), \quad (6)$$

where $B(\alpha, \beta) = \Gamma(\alpha)\Gamma(\beta)/\Gamma(\alpha + \beta)$ is the beta function. This corresponds to

$$\rho_{\pm}(x) = \frac{1}{4^{\gamma/\mu} B(\frac{\gamma}{\mu}, \frac{\gamma}{\mu})} \frac{\mu}{v_0} \left(1 \pm \frac{\mu x}{v_0} \right)^{\frac{\gamma}{\mu}} \left(1 \mp \frac{\mu x}{v_0} \right)^{\frac{\gamma}{\mu} - 1}. \quad (7)$$

Hence the densities are singular at the edges: the total density diverges for $\gamma < \mu$, vanishes for $\gamma > \mu$, and is uniform on the interval $[-x_e, x_e]$ for the marginal case $\gamma = \mu$, with $x_e = v_0/\mu$ in all cases. Note also that the density ρ_+ always vanishes at the left edge, and ρ_- at the right edge.

In this paper we study the $N \rightarrow +\infty$ limit of the model (1) with the harmonic potential (2). The passive case $v_0 = 0$, $T > 0$ was studied in [66], where the stationary density was found to take a scaling form

$$\rho_{\text{eq}}(x) = \frac{\mu}{2\kappa} \hat{\rho}_g \left(x \sqrt{\frac{\mu}{T}} \right), \quad g = \frac{\kappa}{\sqrt{\mu T}}, \quad (8)$$

where $\hat{\rho}_g(y)$ is a smooth function whose support is the whole real axis. As g varies, it interpolates between a Gaussian in the weakly interacting limit $g \rightarrow 0$ and a square density in the small temperature limit $g \rightarrow +\infty$.

Here we focus on the active case $T = 0$, $v_0 > 0$. Using the same method as in [68], we obtain a pair of partial differential equations for the rank fields, defined as

$$r(x, t) = \int_{-\infty}^x dy \rho_s(y, t) - \frac{1}{2}, \quad s(x, t) = \int_{-\infty}^x dy \rho_d(y, t). \quad (9)$$

We focus on the stationary state where $r(x, t) \rightarrow r(x)$ and $s(x, t) \rightarrow s(x)$. We then analyze the stationary equations to extract relevant information on the stationary densities $\rho_s(x) = r'(x)$ and $\rho_d(x) = s'(x)$. Since the potential is even in x , we find stationary solutions with $r(x) \in [-1/2, 1/2]$ an odd function of x , and $s(x)$ an even function of x . Our results are summarized in Fig. 1, which shows the different regimes as a function of the two dimensionless parameters (3), as well as a sketch of the total density $\rho_s(x)$ in each regime.

- In phase I, which extends both for repulsive and attractive interactions, corresponding to $\frac{\mu}{\gamma} < \min(1, 1 + \frac{\kappa}{v_0})$ the total density $\rho_s(x)$ is smooth and vanishes at the edges with an exponent $\frac{\gamma}{\mu} - 1$, similar to the non-interacting case $\kappa = 0$. In fact, all the densities ρ_{\pm} vanish with the same exponents as in the absence of interactions (although with different amplitudes).
- In phase II, which corresponds to the repulsive case with $\mu > \gamma$, the density instead converges to a finite value at the edges, leading to a jump of magnitude

$$\rho_s(x_e) = \frac{\mu - \gamma}{2\kappa}. \quad (10)$$

Hence we find that the repulsive interactions suppress the divergence which is present for $\kappa = 0$. Furthermore, the density ρ_+ still vanishes at the left edge, and ρ_- at the right edge, but they now vanish linearly as $|x \pm x_e|$, instead of superlinearly. The phase II is divided in two regimes IIa and IIb depending on the convexity of the density inside the support. In both phases I and II there are no shocks, and the support is given by $[-x_e, x_e]$ with

$$x_e = \frac{v_0 + \kappa}{\mu}. \quad (11)$$

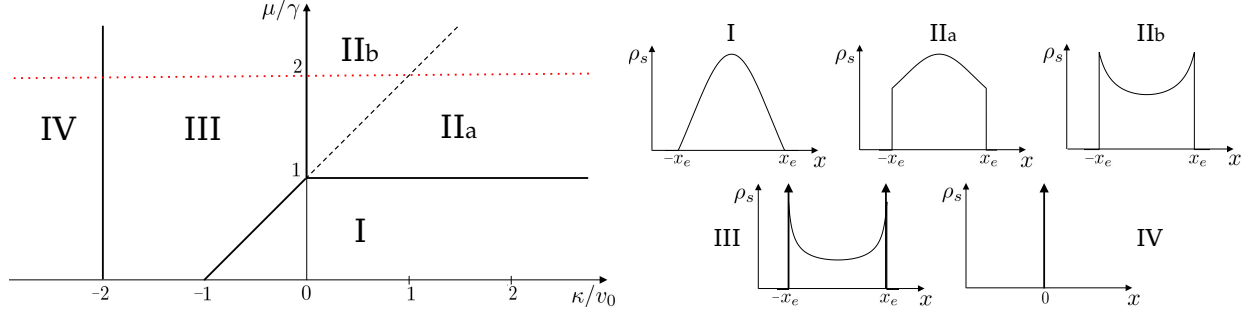


FIG. 1. Left panel: phase diagram of the active jellium model, (i.e. the active rank diffusion in a harmonic potential $V(x) = \frac{\mu}{2}x^2$) in the plane $(\frac{\kappa}{v_0}, \frac{\mu}{\gamma})$, with repulsive interactions for $\kappa > 0$ and attractive for $\kappa < 0$. Right panel : schematic representation of the total density $\rho_s(x)$ for each phase. The up arrows represent delta functions in the density, i.e. shocks/clusters of particles. In phases I, IIa and IIb there are no shocks. In phase I (which extends on either side of $\kappa = 0$) the density vanishes at the edge (with an exponent $\frac{\gamma}{\mu} - 1$ identical to the non-interacting case $\kappa = 0$). In phases IIa and IIb the density has a finite jump at the edge (except for $\kappa = 0$ where it diverges). The dotted line between phases IIa and IIb represents only a crossover where the density changes from concave to convex (not a true phase transition). In phase III there are shocks at the two edges, with a cluster of $+$ only particles at the right edge, and $-$ only at the left edge. In phase IV all the particles belong to a single cluster. In the text more explicit expressions are obtained on the special line $\frac{\mu}{\gamma} = 2$, represented as a dotted red line on the phase diagram.

On the boundary between the regimes I and IIa, i.e. for $\gamma = \mu$, the density vanishes at the edge as

$$\rho_s(x) \simeq \frac{\mu}{2\kappa} \frac{1}{(\ln(x_e - x))^2}. \quad (12)$$

This inverse logarithmic divergence is purely an effect of the interactions, as it occurs only for $\kappa > 0$, while in the non-interacting case the density is uniform for $x \in [-v_0/\mu, v_0/\mu]$ for $\gamma = \mu$.

- Phase III is restricted to the attractive case, for $\frac{\mu}{\gamma} > 1 + \frac{\kappa}{v_0}$ and $-2v_0 < \kappa = -\bar{\kappa} < 0$, and it is characterized by the presence of shocks at the edges, i.e. the density has delta peaks at $\pm x_e$, corresponding to a cluster of $+$ particles at x_e and $-$ particles at $-x_e$. A similar phenomenon was observed both in the absence of a potential, and in the case of the linear potential. An important difference is that here one has $x_e > \frac{v_0 - \bar{\kappa}}{\mu}$, i.e. the support is *extended* by the presence of shocks:

$$x_e = \frac{v_0 - \bar{\kappa}}{\mu} + \frac{\bar{\kappa}p}{2\mu} \quad (13)$$

where p is the total fraction of particles in the two clusters. In the other two cases the support was infinite in the absence of shocks.

- Finally, phase IV corresponds to the case $\kappa < -2v_0$, for which one trivially has $\rho_s(x) = \delta(x)$, i.e. all particles belong to a single cluster, which is stable.

We were also able to take the computations further in the special case $\mu/\gamma = 2$ (the red line in Fig. 1). For $\kappa > v_0$, i.e within phase IIa, the rank field $r(x)$ is obtained in parametric form

$$\frac{\mu x}{v_0} \sinh(c/2) = \tilde{g}_c(r) \quad , \quad \tilde{g}_c(r) := \sinh(cr) + cr \cosh\left(\frac{c}{2}\right), \quad (14)$$

where $c \in [0, +\infty]$ is the solution of

$$\frac{\tanh(c/2)}{c/2} = \frac{v_0}{\kappa}. \quad (15)$$

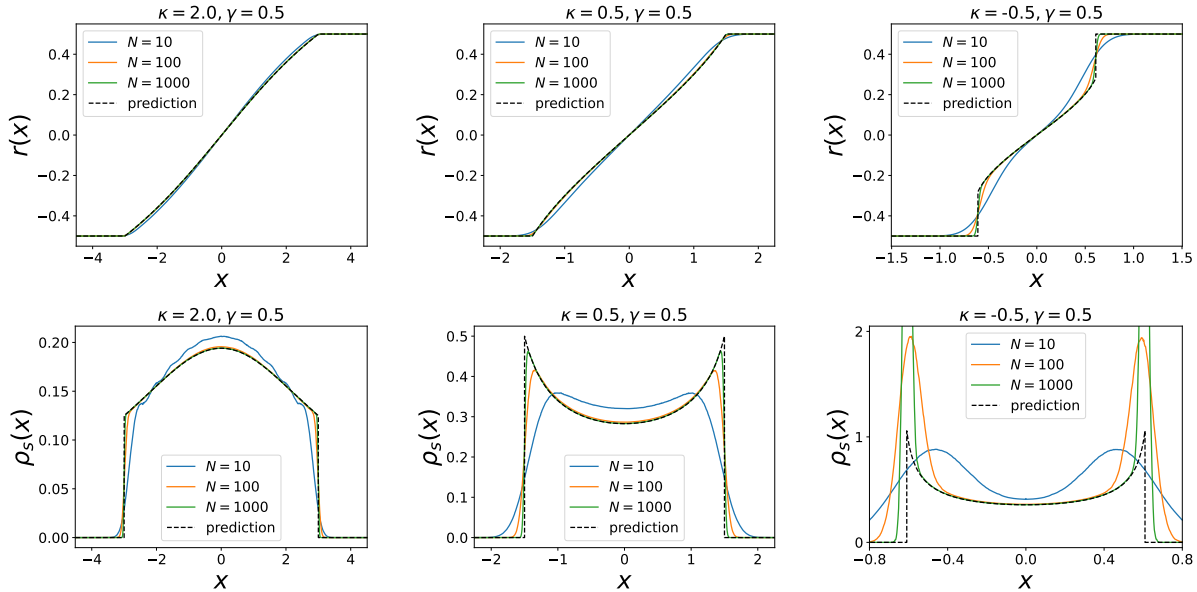


FIG. 2. **Top:** Comparison of the rank field $r(x)$ in the stationary state computed using numerical simulations with different values of N , with the analytical prediction for $a = 1/2$ i.e. $\mu = 2\gamma$. In all cases $v_0 = 1$, $\mu = 1$ and $\gamma = 0.5$, and κ varies to explore the 3 non-trivial regimes: $\kappa > v_0$, i.e. phase IIb (left), $0 < \kappa < v_0$, i.e. phase IIa (center) and $-2v_0 < \kappa < 0$, i.e. phase III (right). In $r(x)$, the shocks appear as jumps for $N \rightarrow +\infty$ in the right panel. The dashed black lines correspond to the predictions of Eqs. (14), (16) and (16)-(17) respectively. **Bottom:** Plot of the density $\rho_s(x) = r'(x)$ for the same parameters, obtained through numerical simulations. The dashed black lines correspond to the prediction (80) (the delta peaks are not shown on the right panel).

Since $\tilde{g}_c(r)$ is an increasing function of r for any value of c , the Eq. (14) is invertible, $r(x)$ is smooth and there is no shock. In that case the edge is given by the general formula (11).

For $\kappa < v_0$, we find instead

$$\frac{\mu x}{v_0} \sin(c/2) = g_c(r) \quad , \quad g_c(r) := \sin(cr) + cr \cos\left(\frac{c}{2}\right) \quad , \quad \frac{\tan(c/2)}{c/2} = \frac{v_0}{\kappa} . \quad (16)$$

In the repulsive case, $\kappa > 0$, i.e. in phase IIb, one has $c \in [0, \pi]$ and $g_c(r)$ is again an increasing function on $[0, 1/2]$, so that this relation can be inverted and there is no shock. The edge is again given by (11). In the attractive case, $\kappa < 0$, i.e. in phase III, one has instead $c \in [\pi, 2\pi]$ and $g_c(r)$ is no longer increasing on the whole interval $[0, 1/2]$. In that case, we find that there is a shock at the edge, i.e. a delta function in the density with weight $\frac{1}{2} - r(x_e^-)$. This weight is determined from the equation

$$h_c(r(x_e^-)) = h_c\left(\frac{1}{2}\right) \quad , \quad h_c(r) = \sin(cr) + \frac{cr}{2} \cos\left(\frac{c}{2}\right) . \quad (17)$$

The position of the edge x_e is then obtained by inserting the value of $r(x_e^-)$ in (16). More details on the derivations and the results are given below.

Another interesting case is the limit $\gamma \ll \mu$. In that limit the system spends most of the time near "fixed points" of the dynamics [48]. We show that in the repulsive case $\kappa > 0$, it results in the following bimodal shape for the total density

$$\rho_s(x) = \frac{\mu}{2\kappa} \quad \text{for} \quad \frac{v_0}{\mu} < |x| < \frac{v_0 + \kappa}{\mu} , \quad (18)$$

i.e. the density exhibits a gap inside which it vanishes. This is explained by the fact that there is a separation between + particles on the right and - on the left.

Finally in the diffusive limit $v_0 \rightarrow +\infty$, $\gamma \rightarrow +\infty$ with $T_a = \frac{v_0^2}{2\gamma}$ fixed one can show (see [68]) from the equations derived below that at large N the total density $\rho_s(x)$ converges to the one of the passive case with $T = T_a$, given in [66].

The above results, valid for $N \rightarrow +\infty$, have been tested by numerical simulations for large values of N . In Fig. 2, the predictions for the rank field $r(x)$ and the total density $\rho_s(x)$ for $\mu = 2\gamma$ in the 3 different regimes are compared with the results obtained by simulating the dynamics of equation (1) and averaging over time, in the stationary state, for different values of N . At finite N the density is always smooth (the jumps and the delta peaks at the edges have a finite width which decreases with N , due in the second case to fluctuations in the size and position of the clusters), but as N increases the agreement with the predictions becomes very good. For more details on the method used for the numerical simulations, see the supplementary material of [68].

In Appendix A, we introduce a variant of the present model with non-reciprocal interactions inspired from the notion of vision cone. The interaction still takes the form of a 1D Coulomb potential, but now each particle only receives a force from the particles "in front" of it (i.e. on the right for + particles and on the left for - particles). It turns out that this model can be mapped to the reciprocal active rank diffusion model studied here in the case of a harmonic confining potential, and in [68] in the absence of confinement or with a linear potential. The full phase diagram for this model with non-reciprocal interactions can thus be directly deduced from the present results and those of our previous work (see Appendix A).

B. Non reciprocal rank interaction

We have also considered more general rank interactions, where the interaction parameter between particle i and particle j depends on their internal states, $\sigma_i(t)$ and $\sigma_j(t)$. It is parameterized by a 2 by 2 matrix of couplings $\kappa_{\sigma,\sigma'}$ with $\sigma = \pm 1$ and $\sigma' = \pm 1$. It is described by the equation of motion

$$\frac{dx_i}{dt} = \frac{1}{N} \sum_{j=1}^N \kappa_{\sigma_i(t),\sigma_j(t)} \text{sgn}(x_i - x_j) - V'(x_i) + v_0 \sigma_i(t). \quad (19)$$

We have specialized to the interesting case of a non-reciprocal interaction such that

$$\kappa_{-+} = -\kappa_{+-} = b \quad , \quad \kappa_{++} = \kappa_{--} = 0. \quad (20)$$

Restricting to $b > 0$ by symmetry, this means that + particles are attracted to - particles, while - particles are repelled by + particles (and two particles with the same sign do not interact together). We find that for any $N \geq 2$ in the absence of external potential the particles eventually escape to infinity and there is no bound stationary state.

We have thus studied the system in presence of a confining linear external potential $V'(x) = a \text{sgn}(x)$, with $a > 0$. Our results are summarized in Fig. 3. We find that there are four phases. The phase IV corresponds to $a \geq v_0 + b/2$ and is trivial: the particles cannot escape from $x = 0$ and the density is thus a single delta peak at $x = 0$. In phases I, II and III the density is smooth outside of $x = 0$ and decays exponentially as $\rho_s(x) \sim e^{-A_+x}$ for $x \rightarrow +\infty$ and $\rho_s(x) \sim e^{A_-x}$ for $x \rightarrow -\infty$. The inverse sizes A_{\pm} of the bound state on the two sides are given below. The asymmetry of the stationary density is a result of the non-reciprocity of the interaction. These three phases differ mainly by their behavior near and at $x = 0$, and by the absence or presence of particles on either side of $x = 0$. In phase I the density exhibits only a jump at $x = 0$, and its support is the whole real line. In phases II and III the density exhibits a delta peak (i.e. a shock, a cluster of + particles) at $x = 0$. In phase II the density vanishes for $x > 0$, i.e. all particles are either in the shock or at the left of $x = 0$. Surprisingly, in phase III the support of the density is again the whole real line. This phase which exists for large non-reciprocity is dominated by fluctuations, see below. Let us now describe each phase in more details.

In phase I, i.e. for $0 < a < v_0 - b/2$, the support of the density is the whole real line. The total density

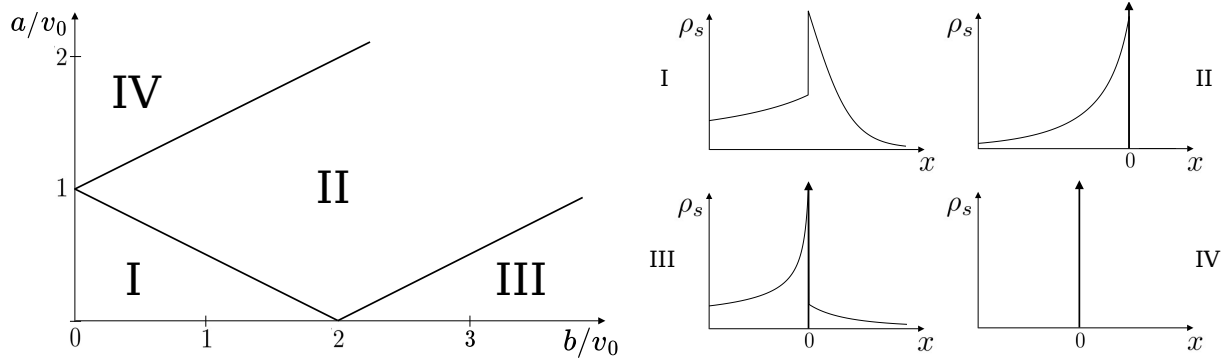


FIG. 3. Left: Phase diagram of the non-reciprocal active rank diffusions. The phase diagram is symmetric upon $b \rightarrow -b$ and a parity transformation $x \rightarrow -x$. Right: the behavior of the total particle density in the four phases. The arrows denote delta function peaks in the density.

reads

$$\rho_s(x) = \begin{cases} A_+ \frac{2v_0 - b}{2b} \left(1 - \frac{1}{1 + W\left(\frac{b}{2v_0} e^{-A_+ x + \frac{b}{2v_0}}\right)} \right) & \text{for } x > 0, \\ \rho_s(x) = A_- \frac{2v_0 + b}{2b} \left(\frac{1}{1 + W\left(-\frac{b}{2v_0} e^{A_- x - \frac{b}{2v_0}}\right)} - 1 \right) & \text{for } x < 0, \end{cases} \quad \text{with } A_{\pm} = \frac{8a\gamma}{(2v_0 \mp b)^2 - 4a^2}, \quad (21)$$

where W is the Lambert function, i.e. the real (and first) root of $W(z)e^{W(z)} = z$. Since $W(z) \simeq z$ at small z , the density decays exponentially at large $|x|$ with rates A_{\pm} . The decay is slower on the negative side for $b > 0$ since then $A_- < A_+$. The density exhibits a discontinuity at $x = 0$

$$\frac{\rho_s(0^-)}{\rho_s(0^+)} = \frac{1 - \frac{4a^2}{(2v_0 - b)^2}}{1 - \frac{4a^2}{(2v_0 + b)^2}}, \quad (22)$$

which is smaller than unity for $b > 0$.

In phase II, i.e. for $v_0 - b/2 < a < v_0 + b/2$, the density $\rho_s(x)$ vanishes for $x > 0$ and it has a delta peak at $x = 0$ with weight

$$\frac{1}{2} - r(0^-) = \frac{2a}{2a + b + 2v_0}, \quad (23)$$

containing only + particles. For $x < 0$ it is given by

$$\rho_s(x) = A_- \frac{2v_0 + b}{2b} \left(\frac{1}{1 + W\left(-\frac{2b}{2a + b + 2v_0} e^{A_- x - \frac{2b}{2a + b + 2v_0}}\right)} - 1 \right), \quad (24)$$

where A_- is still given by (21). One has $\rho_s(0^-) = (b + 2v_0)A_- / (2a - b + 2v_0)$.

Note that A_+ diverges as the phase II is approached from phase I, and all + particles for $x \geq 0$ become part of the cluster at $x = 0$, i.e. the weight (23) is non-zero on the frontier between phase I and phase II and $\rho_s(0^+)$ diverges in that limit.

Finally, in phase III, i.e. for $a < v_0 - b/2$, the density $\rho_s(x)$ is again non zero both for $x > 0$ and $x < 0$ and it has a delta peak at $x = 0$ of weight

$$r(0^+) - r(0^-) = \frac{2a(b^2 - 2ab - 4v_0^2)}{b(b^2 - 4a^2 - 4v_0^2)} \quad (25)$$

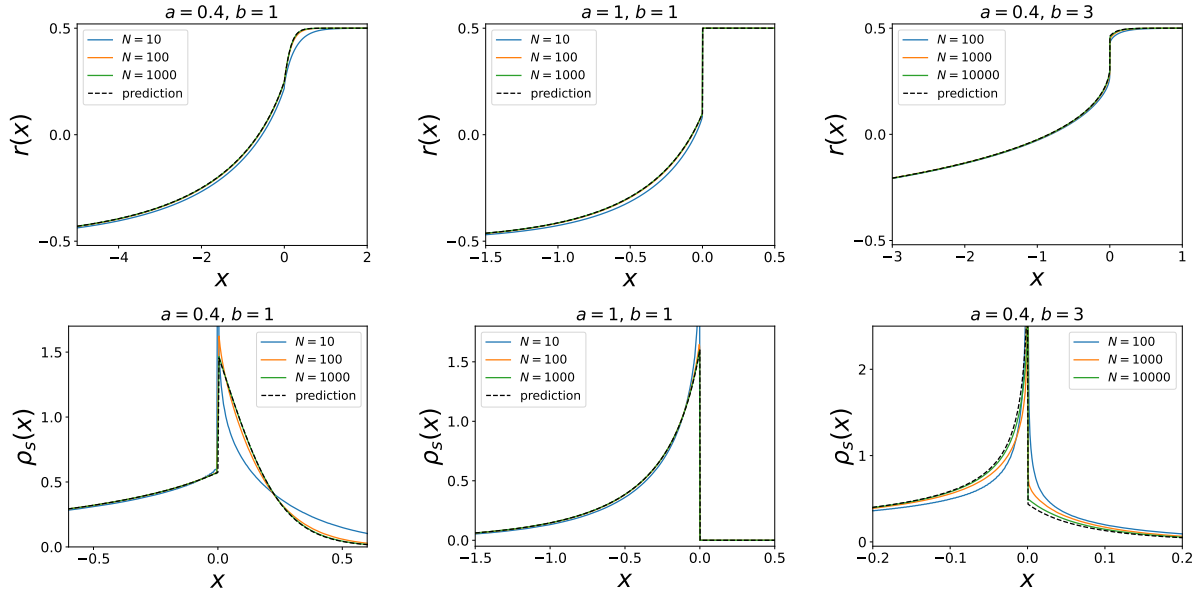


FIG. 4. Rank field $r(x)$ (top) and total density $\rho_s(x) = r'(x)$ (bottom) obtained from simulations with $\gamma = 1$ and $v_0 = 1$, for increasing values of N . The delta peaks are not shown on the densities for the phases II and III, but they are visible as discontinuities in $r(x)$. Left: $a = 0.4$ and $b = 1$ (phase I). The dashed black line corresponds to the prediction for infinite N (21). Note the discontinuity of the density at $x = 0$, with however no shock (no delta peak). Center: $a = 1$ and $b = 1$ (phase II). The dashed black line corresponds to (24). The density is zero for $x > 0$ for any N (with a delta peak at $x = 0$). Right: $a = 0.4$ and $b = 3$ (phase III) the dashed black line corresponds to (26). Larger values of N are used here since the convergence in N is slower than in the other phases.

containing only + particles. For $x \neq 0$ the density is given by

$$\rho_s(x) = \begin{cases} A_+ \frac{b - 2v_0}{2b} \left(\frac{1}{1 + W(-B_+ e^{-A_+ x - B_+})} - 1 \right), & x > 0, \\ \rho_s(x) = A_- \frac{2v_0 + b}{2b} \left(\frac{1}{1 + W(-B_- e^{A_- x - B_-})} - 1 \right), & x < 0, \end{cases} \quad B_{\pm} = \frac{(b \pm 2v_0)(b - 2a \mp 2v_0)}{b^2 - 4a^2 - 4v_0^2}, \quad (26)$$

where A_{\pm} are the same as in (21).

Note again that A_+ diverges as the phase II is approached from phase III. However in this case the fraction of particles on the right side of $x = 0$ vanishes continuously as one approaches this line, i.e. $\frac{1}{2} - r(0^+) \rightarrow 0$. Thus the weight of the delta peaks in the two phases, given by (23) and (25) respectively, match on the frontier between phase III and II (one finds $r(0^+) - r(0^-) = \frac{1}{2} - \frac{v_0}{b}$ in both cases).

These results can be interpreted by considering the force seen by the particles near $x = 0$, due to the combined effect of the potential and the non-reciprocal attractive interaction. In phase I, one finds that all the + particles move towards the right and the - particles towards the left, until they change sign. The total force felt by the rightmost particle, assuming that it is a + particle, is $v_0 - a - b/2$, which is indeed positive inside phase I. When this force becomes negative, this marks the transition to phase II. In this phase, all the + particles are attracted towards $x = 0$, while the - particles still move towards the left. This explains why a cluster of + particles forms at $x = 0$ and no particle can access $x > 0$. The force felt by the leftmost particle, assuming that it is a - particle, is $-v_0 + a - b/2$. When this becomes positive, this marks the transition to phase IV where all particles are attracted towards $x = 0$ indifferently of their sign and remain there. The behaviour of the particles in phase III is less intuitive. In this phase, all the + particles are attracted towards $x = 0$ while the - particles are repelled either towards $x > 0$ or $x < 0$. When a + particle from the cluster at $x = 0$ becomes a - particle, the side towards which it is directed is determined by the

fluctuations. Thus this phase is more sensitive to the fluctuations than the other phases.

The analytical results and the qualitative description above are valid in the limit $N \rightarrow +\infty$. In Fig. 4 we compare our analytical predictions for $r(x)$ and $\rho_s(x)$ for $N \rightarrow +\infty$ to numerical results obtained through simulations of the stochastic dynamics of equation (19) and averaging over time, in the stationary state, for finite values of N . We observe that the 4 phases already exist for finite N , with the same qualitative behaviours (presence of a true delta peak at $x = 0$, absence or presence of a smooth density of particles on the right...). The quantitative values differ from our predictions for small values of N , but rapidly converge as $N \rightarrow +\infty$. In phase IV the convergence is slower due to the peculiar role played by the fluctuations in this phase, as discussed above.

C. Outline of the paper

In the rest of the paper we give the derivations for all the results presented here. In Section III we study active rank diffusions in a harmonic trap. We start by deriving the general equations for the model and we obtain a parametric representation of the stationary densities in the large N limit. After recalling the non-interacting case, we first study the special line $\mu = 2\gamma$ in the phase diagram for which a more explicit solution can be obtained. Then we consider the general case and use the previously obtained representation to study the presence or absence of shocks and the edge behavior of the densities. We finally discuss in detail the phase diagram, and conclude with a study of the limit of small γ . In Section IV we consider the case of RTP's with non-reciprocal rank interactions. We first derive the general equations for arbitrary non-reciprocal rank interactions between the \pm states. We specialize to a simple version of the model presented above and derive the exact densities in the large N limit. We then examine the three non-trivial phases in detail and obtain the phase diagram.

III. ACTIVE RANK DIFFUSIONS IN A HARMONIC TRAP

A. General equations for the rank fields

Using the Dean-Kawasaki approach [89, 90], one can establish starting from (1), as in [66] and [48], an exact stochastic evolution equation for the density fields, which takes the following form

$$\partial_t \rho_\sigma = T \partial_x^2 \rho_\sigma + \partial_x \rho_\sigma (-v_0 \sigma + V'(x) + \bar{\kappa} \int dy \rho_s(y, t) \text{sgn}(x - y)) + \gamma \rho_{-\sigma} - \gamma \rho_\sigma + O\left(\frac{1}{\sqrt{N}}\right), \quad (27)$$

where the $O(\frac{1}{\sqrt{N}})$ term represents the passive and active noises, see Supp. Mat. in [68], and Sec. III A of [48]. It is convenient to define, as in [66, 68], the rank fields

$$r(x, t) = \int_{-\infty}^x dy \rho_s(y, t) - \frac{1}{2}, \quad s(x, t) = \int_{-\infty}^x dy \rho_a(y, t). \quad (28)$$

Focusing from now on on the large N limit, and henceforth neglecting the noise terms in (27), one obtains from (27) and (28) two coupled deterministic differential equations (see [68])

$$\partial_t r = T \partial_x^2 r - v_0 \partial_x s + 2\bar{\kappa} r \partial_x r + V'(x) \partial_x r, \quad (29)$$

$$\partial_t s = T \partial_x^2 s - v_0 \partial_x r + 2\bar{\kappa} r \partial_x s + V'(x) \partial_x s - 2\gamma s. \quad (30)$$

These equations are valid both for the attractive and the repulsive case. Since $\rho_s(x, t)$ is positive and normalized to 1, $r(x, t)$ must be an increasing function with $r(\pm\infty, t) = \pm\frac{1}{2}$. One sees that $\partial_t s(+\infty, t) = -2\gamma s(+\infty, t)$, hence at large time $s(\pm\infty, t) = 0$. In the passive case $v_0 = 0$ the first equation recovers Burger's equation which describes usual rank diffusion [66]. One generally expects that in the diffusive limit $v_0, \gamma \rightarrow +\infty$ with $T_a = \frac{v_0^2}{2\gamma}$ fixed, RTP's behave as Brownian particles. This also holds here. Indeed, in (30) only two terms remain relevant in that limit, and one obtains $s \simeq -\frac{v_0}{2\gamma} \partial_x r$. Inserting in (29)

the active term $-v_0 \partial_x s(x, t)$ becomes $T_a \partial_x^2 r(x, t)$, i.e. a diffusive thermal term with effective temperature T_a .

In the remainder of the paper we will only consider RTP noise, setting $T = 0$.

B. A parametric representation for the stationary state in a general confining potential

We start from the stationary Dean-Kawasaki equation (i.e. with time derivatives set to zero) for an arbitrary confining external potential $V(x)$,

$$\begin{aligned} 0 &= -v_0 s' - 2\kappa r r' + V'(x) r' , \\ 0 &= -v_0 r' - 2\kappa r s' - 2\gamma s + V'(x) s' \end{aligned} \quad (31)$$

(where the primes now denote spatial derivatives), which must be solved with boundary conditions $r(\pm\infty) = \pm\frac{1}{2}$ and $s(\pm\infty) = 0$. Let us recall that $\kappa > 0$ corresponds to repulsive interaction, while $\kappa = -\bar{\kappa} < 0$ corresponds to attractive interaction. The function $r(x)$ is increasing, but may have plateaus or jumps (shocks) at some positions. On each interval where $r(x)$ is strictly monotonous and smooth, it is always possible to write

$$V'(x) = W'(r(x)) \quad (32)$$

and hope to determine $V(x)$ from $W(r)$ later on. Integrating the first equation one obtains

$$s = \frac{1}{v_0} \left(-\kappa \left(r^2 - \frac{1}{4} \right) + W(r) \right) , \quad (33)$$

where $W(r)$ should satisfy some boundary conditions, including $W(\pm\frac{1}{2}) = 0$. We introduce

$$U(r) = -\kappa \left(\frac{1}{4} - r^2 \right) - W(r) \quad , \quad s = -U(r)/v_0 \quad , \quad U(\pm\frac{1}{2}) = 0 . \quad (34)$$

The second equation in (31) becomes

$$(v_0^2 - U'(r)^2) r' = 2\gamma U(r) . \quad (35)$$

Integrating this equation, and restricting for convenience to potentials $V(x)$ which are even in x , such that $r(x)$ is odd, and $r(0) = 0$ (assuming that there is no shock at $x = 0$) one finds an equivalent parametric representation of Eqs. (31) in the form

$$x = \int_0^{r(x)} dr \frac{v_0^2 - U'(r)^2}{2\gamma U(r)} , \quad (36)$$

$$-V'(x) = -2\kappa r + U'(r) , \quad (37)$$

together with $s = -U(r)/v_0$. It is parametric in the sense that for any choice of $U(r)$ one obtains in principle a solution $(r(x), s(x))$ of Eqs. (31) for "some" potential $V(x)$ determined a posteriori.

C. A general class of solutions for the harmonic potential

We now specialize to a harmonic external potential $V'(x) = \mu x$. In this case if the solution is unique, $r(x)$ is odd, and $s(x)$ is even in x . We apply the method of the previous subsection. Eq. (37) becomes

$$\mu x = 2\kappa r - U'(r) . \quad (38)$$

We will first determine $U(r)$, which will allow for finding $r(x)$ through the above equation. To this aim, let us replace x using (36) and take the derivative with respect to r . We obtain

$$U''(r) - 2\kappa + \mu \frac{v_0^2 - U'(r)^2}{2\gamma U(r)} = 0, \quad (39)$$

which can be rewritten as

$$U'(r)^2 - v_0^2 = 2aU(r)U''(r) - bU(r) \quad \text{with } a = \frac{\gamma}{\mu} \text{ and } b = 4a\kappa. \quad (40)$$

This equation can be solved parametrically by introducing the function $g(u)$ such that $g(U(r)) = U'(r)$. This implies that $U'' = g'(U)U' = g'(U)g(U)$, and thus $g(u)$ satisfies

$$g^2(u) - v_0^2 = 2aug(u)g'(u) - bu. \quad (41)$$

Introducing $G(u) = g^2(u)$ we finally obtain

$$auG'(u) - G(u) - bu + v_0^2 = 0, \quad (42)$$

for which the solutions are

$$G(u) = \begin{cases} Cu^{1/a} + \frac{b}{a-1}u + v_0^2 & \text{for } a \neq 1, \\ Cu + bu \ln u + v_0^2 & \text{for } a = 1, \end{cases} \quad (43)$$

with C a constant to be determined.

We now have to solve $(U')^2 = G(U)$. Hence we need to know the sign of $U'(r)$. Since from (34) we have that $s = -U(r)/v_0$, and we expect that in the stationary state there is a surplus of $-$ particles for $x < 0$ and $+$ particles for $x > 0$. Hence $s(x)$ should be negative, with $s(\pm\infty) = 0$ and a minimum at $x = 0$. Since $r(x)$ is an increasing function with $r(0) = 0$, this suggests that $U(r)$ should have a maximum at $r = 0$. Hence $U'(r)$ should be positive for $r < 0$ and negative for $r > 0$, with $U'(0) = 0$ (the last point can also be deduced from (37) with $V'(x) = \mu x$, since $r(0) = 0$ by symmetry). This leads to

$$U' = -\text{sgn}(r)\sqrt{G(U)} \quad , \quad U'(0) = 0. \quad (44)$$

The second property will allow to determine the constant C (see below). Since $r(x)$ is an odd function of x , from now on we will focus on $r > 0$ and $x > 0$. Using the boundary condition in (34), $U(\frac{1}{2}) = 0$, we thus obtain a parametric equation for $U(r)$, which together with (38), also determines $r(x)$

$$\frac{1}{2} - r = \int_0^{U(r)} \frac{du}{\sqrt{G(u)}}, \quad (45)$$

$$\mu x = 2\kappa r - U'(r), \quad (46)$$

where $G(U)$ is given in (43). The constant C is fixed by the condition $G(U(0)) = 0$, i.e. denoting $u_0 = U(0)$,

$$C = \begin{cases} -\frac{b}{a-1}u_0^{1-\frac{1}{a}} - v_0^2u_0^{-1/a} & \text{for } a \neq 1, \\ -b \ln u_0 - \frac{v_0^2}{u_0} & \text{for } a = 1. \end{cases} \quad (47)$$

where u_0 is the solution of

$$\frac{1}{2} = I(u_0) \quad , \quad I(u_0) := \begin{cases} u_0 \int_0^1 \frac{dw}{\sqrt{v_0^2(1-w^{1/a}) + \frac{bu_0}{a-1}(w-w^{1/a})}} & \text{for } a \neq 1, \\ u_0 \int_0^1 \frac{dw}{\sqrt{v_0^2(1-w) + bu_0 w \ln w}} & \text{for } a = 1, \end{cases} \quad (48)$$

which has been obtained taking $r = 0$ in (45) and noting that one can rewrite, with $u_0 = U(0)$,

$$G(u) = \begin{cases} v_0^2 \left(1 - \left(\frac{u}{u_0} \right)^{1/a} \right) + \frac{bu_0}{a-1} \left(\frac{u}{u_0} - \left(\frac{u}{u_0} \right)^{1/a} \right) & \text{for } a \neq 1, \\ v_0^2 \left(1 - \frac{u}{u_0} \right) + bu \ln \frac{u}{u_0} & \text{for } a = 1. \end{cases} \quad (49)$$

In the repulsive case, $b > 0$, an analysis of the argument of the square root in (48) shows that for any $a > 0$, $I(u_0)$ is a strictly increasing function of $u_0 \in [0, u_0^{\max}]$, which diverges as $u_0 \rightarrow u_0^{\max} = v_0^2/b$, and evaluates to 0 at $u_0 = 0$. In the attractive case, $b < 0$, one has the same result with $u_0^{\max} = +\infty$. Thus there always exists a unique value of $u_0 > 0$ for which (48) is satisfied. Once $G(u)$ is known, this leads to a parametric representation for $r(x)$ obtained by varying $U \in [0, u_0]$

$$r = \frac{1}{2} - \int_0^U \frac{du}{\sqrt{G(u)}}, \quad (50)$$

$$\mu x = \kappa - 2\kappa \int_0^U \frac{du}{\sqrt{G(u)}} + \sqrt{G(U)}, \quad (51)$$

where $G(U)$ is given in (43). One can also obtain a similar representation for $\rho_s(x)$. Taking the derivative of (38) w.r.t. x yields

$$\rho_s(x) = \frac{\mu}{2\kappa - U''(r)}, \quad (52)$$

where, using (44), one has

$$U''(r) = -\frac{U'(r)G'(U(r))}{2\sqrt{G(U(r))}} = \frac{1}{2}G'(U(r)), \quad (53)$$

with

$$G'(u) = \begin{cases} \frac{C}{a}u^{\frac{1}{a}-1} + \frac{b}{a-1} = -\frac{1}{a} \left(\frac{v_0^2}{u_0} + \frac{b}{a-1} \right) \left(\frac{u}{u_0} \right)^{\frac{1}{a}-1} + \frac{b}{a-1} & \text{for } a \neq 1, \\ C + b(1 + \ln u) = b \ln \frac{u}{u_0} + b - \frac{v_0^2}{u_0} & \text{for } a = 1. \end{cases} \quad (54)$$

To obtain a parametric representation of the density one thus should again vary $U \in [0, u_0]$ and compute

$$\rho_s = \frac{\mu}{2\kappa - \frac{1}{2}G'(U)}, \quad (55)$$

$$\mu x = \kappa - 2\kappa \int_0^U \frac{du}{\sqrt{G(u)}} + \sqrt{G(U)}. \quad (56)$$

Note that all the results derived in this subsection are valid both for repulsive ($\kappa > 0$) and attractive ($\kappa < 0$) interactions, as long as there are no shocks. The condition for the absence of shocks will be studied below. We will now examine this general solution in more details, starting with the non interacting case $\kappa \rightarrow 0$, then the repulsive case, and finally the attractive case (where the shocks can occur).

D. Non-interacting case $\kappa = 0$

For $\kappa = 0$, the above formulas recover the known result for the density of a stationary RTP in a harmonic potential (see e.g. [12]). Indeed in this case one has $b = 0$, and thus

$$\frac{1}{2} - r = \int_0^{U(r)} \frac{du}{v_0 \sqrt{1 - \left(\frac{u}{u_0} \right)^{1/a}}} = \frac{U(r)}{v_0} {}_2F_1 \left(\frac{1}{2}, a; a+1; \left(\frac{U(r)}{u_0} \right)^{1/a} \right). \quad (57)$$

The equation (48) for u_0 is solved by

$$u_0 = \frac{v_0}{2\sqrt{\pi}} \frac{\Gamma(a + \frac{1}{2})}{\Gamma(a + 1)}. \quad (58)$$

One the other hand one has

$$\mu x = -U'(r) = \sqrt{G(U(r))} = v_0 \sqrt{1 - \left(\frac{U(r)}{u_0}\right)^{1/a}}, \quad (59)$$

which leads to

$$U(r(x)) = u_0 \left(1 - \left(\frac{\mu x}{v_0}\right)^2\right)^a. \quad (60)$$

This implies

$$\frac{1}{2} - r = \frac{u_0}{v_0} \left(1 - \left(\frac{\mu x}{v_0}\right)^2\right)^a {}_2F_1\left(\frac{1}{2}, a; a + 1; 1 - \left(\frac{\mu x}{v_0}\right)^2\right). \quad (61)$$

Taking a derivative and replacing $a = \frac{\gamma}{\mu}$, one finally obtains

$$\rho_s(x) = \frac{2\gamma u_0}{v_0^2} \left(1 - \left(\frac{\mu x}{v_0}\right)^2\right)^{\frac{\gamma}{\mu}-1} = \frac{2}{4\gamma/\mu B(\frac{\gamma}{\mu}, \frac{\gamma}{\mu})} \frac{\mu}{v_0} \left(1 - \left(\frac{\mu x}{v_0}\right)^2\right)^{\frac{\gamma}{\mu}-1}, \quad (62)$$

where $B(\alpha, \beta) = \Gamma(\alpha)\Gamma(\beta)/\Gamma(\alpha + \beta)$ is the beta function, and we have used the identity $B(\alpha, \alpha) = 2^{1-2\alpha}B(\frac{1}{2}, \alpha)$. Using $s = -U(r)/v_0$ and taking the derivative w.r.t x one also finds

$$\rho_d(x) = \frac{\mu x}{v_0} \rho_s(x), \quad (63)$$

which leads to

$$\rho_{\pm}(x) = \frac{1}{4\gamma/\mu B(\frac{\gamma}{\mu}, \frac{\gamma}{\mu})} \frac{\mu}{v_0} \left(1 \pm \frac{\mu x}{v_0}\right)^{\frac{\gamma}{\mu}} \left(1 \mp \frac{\mu x}{v_0}\right)^{\frac{\gamma}{\mu}-1}. \quad (64)$$

E. Special case $a = 1/2$, i.e. $\mu = 2\gamma$

We start with the case $a = 1/2$ which can be solved in a more explicit form (in that case C is dimensionless). We first present the solution assuming that there are no shocks. These solutions will be fully valid in the repulsive case $\kappa > 0$. In the attractive case $\kappa < 0$ we find that there are always shocks, however the above solution is still valid in some range of values of r or x .

1. *Solution in the absence of shocks and repulsive case $\kappa > 0$*

We start by determining the function $U(r)$. In the particular case $a = 1/2$, the integral in (45) can be computed, yielding

$$\begin{aligned} \frac{1}{2} - r &= \left[-\frac{1}{\sqrt{C}} \operatorname{arcsinh} \left(\sqrt{\frac{C^2}{v_0^2 C - b^2}} \left(\frac{b}{C} - u \right) \right) \right]_0^{U(r)} && \text{if } C > \frac{b^2}{v_0^2}, \\ \frac{1}{2} - r &= \left[-\frac{1}{\sqrt{C}} \operatorname{arcosh} \left(\sqrt{\frac{C^2}{b^2 - v_0^2 C}} \left(\frac{b}{C} - u \right) \right) \right]_0^{U(r)} && \text{if } 0 < C < \frac{b^2}{v_0^2}, \\ \frac{1}{2} - r &= \left[-\frac{1}{\sqrt{|C|}} \operatorname{arcsin} \left(\sqrt{\frac{C^2}{b^2 - v_0^2 C}} \left(\frac{b}{C} - u \right) \right) \right]_0^{U(r)} && \text{if } C < 0, \end{aligned} \quad (65)$$

with $C = \frac{2b}{u_0} - \frac{v_0^2}{u_0^2}$,

where we recall that $u_0 = U(0)$ is solution of (48), although we do not need to determine it here (see below). Note that in this case one has $b = 2\kappa$. For now the sign of b is still arbitrary.

Let us consider first the subcase $C > 0$, which corresponds to the first two equations in (65). Inverting the relations (65), and denoting $C = c^2$ ($c > 0$) one obtains

$$U(r) = \frac{1}{c^2} \left(2\kappa \left(1 - \cosh(c(\frac{1}{2} - r)) \right) + cv_0 \sinh(c(\frac{1}{2} - r)) \right). \quad (66)$$

One can check that it satisfies $U(1/2) = 0$ and that it obeys (40). The condition $G(U(0)) = 0$ is then equivalent to

$$\frac{\tanh(c/2)}{c/2} = \frac{v_0}{\kappa}. \quad (67)$$

which determines c . It has a solution only for $\kappa > v_0$, in which case c takes values from $c = 0$ for $\kappa = v_0$ to $c \rightarrow +\infty$ for $v_0/\kappa = 0$.

Let us now discuss the subcase $C < 0$, which corresponds to $\kappa < v_0$. Then one should use the third equation (65) with $C < 0$. Denoting now $C = -c^2$ ($c > 0$), we obtain

$$U(r) = \frac{1}{c^2} \left(-2\kappa \left(1 - \cos(c(\frac{1}{2} - r)) \right) + cv_0 \sin(c(\frac{1}{2} - r)) \right), \quad (68)$$

and $G(U(0)) = 0$ is now equivalent to

$$\frac{\tan(c/2)}{c/2} = \frac{v_0}{\kappa}, \quad (69)$$

in which case c varies from $c = 0$ for $\kappa = v_0$ to $c = \pi$ for $v_0/\kappa \rightarrow +\infty$.

We now determine the rank field $r(x)$. We start with the special case $\kappa = v_0$, which corresponds to $c = 0$. Taking the limit, one obtains

$$U(r) = -\frac{1}{8}(2r - 1)(2\kappa(2r - 1) + 4v_0) = v_0 \left(\frac{1}{4} - r^2 \right). \quad (70)$$

This quadratic function is a solution of (40) for any κ and v_0 , but it satisfies $U'(0) = 0$ only for $\kappa = v_0$. In this case (46) simply becomes

$$\mu x = 4\kappa r. \quad (71)$$

Thus we obtain, for $\mu = 2\gamma$ and $\kappa = v_0$, the very simple solution

$$r(x) = \frac{\mu x}{4\kappa} \quad \text{for } x \in \left[-\frac{2\kappa}{\mu}, \frac{2\kappa}{\mu}\right], \quad (72)$$

i.e. the total density $\rho_s(x) = \frac{\mu}{4\kappa}$ is constant on the support $\left[-\frac{2\kappa}{\mu}, \frac{2\kappa}{\mu}\right]$. Then one has

$$s(x) = -\frac{U(r(x))}{v_0} = r(x)^2 - \frac{1}{4} = \frac{\mu^2 x^2}{16\kappa^2} - \frac{1}{4}, \quad (73)$$

and thus $\rho_d(x) = \frac{\mu^2 x}{8\kappa^2}$ for $x \in \left[-\frac{2\kappa}{\mu}, \frac{2\kappa}{\mu}\right]$.

Let us now consider the case where $\kappa < v_0$. We substitute $\kappa = \frac{v_0 c}{2 \tan(c/2)}$, from (69). Then the solution (68) reads

$$U(r) = \frac{v_0}{c^2} \left(-\frac{c}{\tan(c/2)} \left(1 - \cos\left(c\left(\frac{1}{2} - r\right)\right) \right) + c \sin\left(c\left(\frac{1}{2} - r\right)\right) \right), \quad (74)$$

which satisfies $G(U(0)) = 0$. The rank field is obtained by inverting

$$\mu x = 2\kappa r - U'(r) = 2\kappa r + v_0 \frac{\sin(cr)}{\sin(c/2)}. \quad (75)$$

Replacing again $\kappa = \frac{v_0 c}{2 \tan(c/2)}$ in (75) one obtains $r(x)$ by inverting

$$\frac{\mu x}{v_0} \sin(c/2) = g_c(r) \quad , \quad g_c(r) := \sin(cr) + cr \cos\left(\frac{c}{2}\right) \quad , \quad \frac{\tan(c/2)}{c/2} = \frac{v_0}{\kappa}, \quad (76)$$

where now c is the only parameter (up to a rescaling of x).

From now on we restrict to the repulsive case $\kappa > 0$, so that c varies between 0 and π . For $c \in [0, \pi]$, $g_c(r)$ is an increasing function on $[0, 1/2]$, so that this relation can be inverted without any issue (i.e. there is no shock). The density has a finite support $[-x_e, x_e]$ where the value of the edge x_e is obtained by taking $r = 1/2$ in (75),

$$x_e = \frac{v_0 + \kappa}{\mu}. \quad (77)$$

For $\kappa > v_0$, one has

$$\mu x = 2\kappa r - U'(r) = 2\kappa r + v_0 \frac{\sinh(cr)}{\sinh(c/2)} \quad , \quad \frac{\tanh(c/2)}{c/2} = \frac{v_0}{\kappa}, \quad (78)$$

or equivalently $r(x)$ is obtained by inverting

$$\frac{\mu x}{v_0} \sinh(c/2) = \tilde{g}_c(r) \quad , \quad \tilde{g}_c(r) = \sinh(cr) + cr \cosh\left(\frac{c}{2}\right) \quad , \quad \frac{\tanh(c/2)}{c/2} = \frac{v_0}{\kappa}, \quad (79)$$

where $c \in [0, +\infty]$. Again $\tilde{g}_c(r)$ is an increasing function so that there is no shock, and the edge is again given by (116) (which as we will see below is a general result in the absence of shocks).

The total density ρ_s can be obtained parametrically by taking the derivative of (76)-(79) w.r.t. x . One should first solve for c and then plot, for $r \in [-1/2, 1/2]$

$$\rho_s = \frac{\mu}{v_0} \frac{\sin(c/2)}{g'_c(r)} \quad , \quad x = \frac{v_0}{\mu} \frac{g_c(r)}{\sin(c/2)}, \quad (80)$$

for $\kappa < v_0$, and the same expression for $\kappa > v_0$ with g_c replaced by \tilde{g}_c and the sine function replaced by a sinh. Similarly one obtains $s(x)$ parametrically from $s = -U(r)/v_0$. This leads to $\rho_d = -U'(r)\rho_s/v_0$, i.e.

$$\rho_d = \frac{\mu}{v_0} \frac{\sin(cr)}{g'_c(r)} \quad , \quad x = \frac{v_0}{\mu} \frac{g_c(r)}{\sin(c/2)}, \quad (81)$$

for $\kappa < v_0$, with the same replacement as above for $\kappa > v_0$.

Behavior at the edge. Let us now see how these densities behave near the edge. Writing $r = \frac{1}{2} - \epsilon$, one has in the case $\kappa < v_0$, $g_c'(\frac{1}{2} - \epsilon) = 2c \cos(c/2) + \epsilon c^2 \sin(c/2)$, which inserting in (80) leads to

$$\rho_s \simeq \frac{\mu}{v_0} \frac{1}{\frac{2c}{\tan(c/2)} + \epsilon c^2} \simeq \frac{\mu}{v_0} \frac{1}{\frac{4\kappa}{v_0} + \epsilon c^2} \simeq \frac{\mu}{4\kappa} \left(1 - \frac{c^2 v_0}{4\kappa} \epsilon \right) \quad (82)$$

(for $\kappa > v_0$ the correction term has a + sign instead). Using that for $r \rightarrow 1/2$, $r \simeq \frac{1}{2} - \rho_s(x_e)(x_e - x)$, we obtain, for any v_0 and κ ,

$$\rho_s(x) \simeq \frac{\mu}{4\kappa} \left(1 + \frac{C v_0 \mu}{16\kappa^2} (x_e - x) \right) . \quad (83)$$

For any v_0 and κ , the density $\rho_s(x)$ has a finite limit at the edge. However, the behavior in the bulk differs in the two cases. When $\kappa < v_0$, C is negative and thus the density has (local) maxima at the edges of the support. Instead, when $\kappa > v_0$, the edges are (local) minima. Recall that in the non-interacting case, for $a = \gamma/\mu = 1/2$, the density has square root divergences at the edges. For $0 < \kappa < v_0$, there is no divergence but there is still an accumulation of particle near the edge. However when $\kappa > v_0$, the interaction "hides" the effect of the activity and we do not observe an accumulation of particles at the edges anymore.

Performing a similar expansion for $\rho_d(x)$ and using $\rho_{\pm} = \frac{\rho_s \pm \rho_d}{2}$ we obtain

$$\begin{aligned} \rho_+(x) &\simeq \frac{\mu}{4\kappa} \left(1 + \left(\frac{C v_0 \mu}{16\kappa^2} - \frac{\mu}{4v_0} \right) (x_e - x) \right) , \\ \rho_-(x) &\simeq \frac{\mu^2}{16v_0\kappa} (x_e - x) . \end{aligned} \quad (84)$$

Thus there are only + particles at x_e (resp. - particles at $-x_e$), while $\rho_-(x)$ vanishes linearly at the edge.

2. Attractive case $\kappa = -\bar{\kappa} < 0$

We now consider the case where $b = -2\bar{\kappa} < 0$. The results of the previous section for $C = -c^2 < 0$ still hold in this case, i.e. one has

$$\frac{\mu x}{v_0} \sin(c/2) = g_c(r) \quad , \quad g_c(r) = \sin(cr) + cr \cos\left(\frac{c}{2}\right) \quad , \quad \frac{\tan(c/2)}{c/2} = -\frac{v_0}{\bar{\kappa}} , \quad (85)$$

where now c varies between π for $v_0/\bar{\kappa} \rightarrow +\infty$ and 2π for $v_0/\bar{\kappa} = 0$. We now need to study the function $g_c(r)$ for $r \in [0, 1/2]$ and for $c \in [\pi, 2\pi]$. It increases as $\sim (1 + \cos(\frac{c}{2}))cr$ at small r , up to $r = r_c = \frac{\pi}{c} - \frac{1}{2}$ where it has a maximum of value

$$g_c(r_c) = g_c^* = \sin\left(\frac{c}{2}\right) + \left(\pi - \frac{c}{2}\right) \cos\left(\frac{c}{2}\right) . \quad (86)$$

Since $r_c < 1/2$ for $c > \pi$ we see that there is always a shock in the attractive case: in order for $r(x)$ to be monotonous, it should have a discontinuity at the edge such that $r(x_e^-) < 1/2$ and $r(x_e^+) = 1/2$. This means that x_e is not necessarily equal to $\frac{v_0 - \bar{\kappa}}{\mu}$ (in fact it is always *larger*, see below) and the density has delta peaks at $\pm x_e$. Since the shock should occur before (or at) the maximum of the curve $g_c(r)$, we obtain the bounds

$$r(x_e^-) \leq r_c \quad , \quad \frac{\mu x_e}{v_0} \sin(c/2) = g(r(x_e^-)) \leq g_c^* . \quad (87)$$

Let us now determine the position of the shock. First of all, note that when $\bar{\kappa} \geq 2v_0$, the noise is not able to compete with the attraction between particles, and the density is simply a delta peak at $x = 0$ (i.e.

$x_e = 0$ in this case). As explained in [68], in the presence of shocks the equations (31) should be interpreted as

$$v_0 s'(x) = \bar{\kappa} [r(x^+) + r(x^-)] r'(x) + V'(x) r'(x), \quad (88)$$

$$v_0 r'(x) = \bar{\kappa} [r(x^+) + r(x^-)] s'(x) - 2\gamma s(x) + V'(x) s'(x). \quad (89)$$

Integrating between x_e^- and x_e^+ this leads to,

$$v_0 \Delta s = \bar{\kappa} (r(x_e^-) + r(x_e^+)) \Delta r + \mu x_e \Delta r, \quad (90)$$

$$v_0 \Delta r = \bar{\kappa} (r(x_e^-) + r(x_e^+)) \Delta s + \mu x_e \Delta s,$$

where $\Delta r = r(x_e^+) - r(x_e^-)$ and similarly for Δs . This implies $\Delta r = \Delta s$ and

$$v_0 = \bar{\kappa} (r(x_e^-) + r(x_e^+)) + \mu x_e, \quad (91)$$

i.e.

$$\frac{\mu x_e}{v_0} = 1 - \frac{\bar{\kappa}}{v_0} \left(\frac{1}{2} + r(x_e^-) \right). \quad (92)$$

Eq. (92) holds for any a . Setting $r(x_e^-) \rightarrow 1/2$ in this equation one recovers the value of the edge in the absence of shock, namely $x_e = x_e^0 = \frac{v_0 - \bar{\kappa}}{\mu}$. Now in presence of a shock, since $r(x_e^-) < 1/2$ one has that $x_e > x_e^0$. Thus because of the presence of the shock the gas can expand further. This is a general result valid for any a , which is in contrast with the behavior both in the absence of external potential and for a linear potential, where the support was infinite in the absence of shocks. It arises here because the restoring force increases with the distance to the origin. When a cluster forms, the attraction felt by the edge particles is reduced and x_e increases so that this is compensated by the external force.

This result can also be obtained through a physical argument, by assuming that there is a cluster of particles at position x_e containing a fraction $\Delta r = \frac{1}{2} - r(x_e^-)$ of particles, all in the $+$ state and writing the condition for dynamical equilibrium is

$$v_0 - \mu x_e - \bar{\kappa} (1 - \Delta r) = 0. \quad (93)$$

Going back to $a = 1/2$ and combining with (85) to eliminate x_e and the parameters other than c , one obtains

$$\frac{g_c(r(x_e^-))}{\sin(c/2)} = 1 - \frac{\bar{\kappa}}{v_0} \left(\frac{1}{2} + r(x_e^-) \right) = 1 + \frac{c}{2 \tan(c/2)} \left(\frac{1}{2} + r(x_e^-) \right), \quad (94)$$

and thus $r(x_e^-)$ is determined by

$$h_c(r(x_e^-)) = h_c\left(\frac{1}{2}\right) \quad , \quad h_c(r) = \sin(cr) + \frac{cr}{2} \cos\left(\frac{c}{2}\right), \quad (95)$$

where we recall that $c \in [\pi, 2\pi]$. The function $h_c(r)$ increases at small r (with $h_c(0) = 0$) and has a maximum at $r_{\max} < \frac{1}{2}$ for any $c \in [\pi, 2\pi]$. Thus, (95) has a solution as long as $h_{c^*}(\frac{1}{2}) > 0$, i.e. for any $\pi < c < c^* = 4.57786\dots$, where c^* is solution of $h_{c^*}(\frac{1}{2}) = 0$, i.e.

$$\frac{\tan(c^*/2)}{c^*/2} = -\frac{1}{2}, \quad (96)$$

which is consistent with the condition $\bar{\kappa} < 2v_0$ (for $\bar{\kappa} \geq 2v_0$ the density is a delta peak, as mentioned above). Eq. (95) allows to determine the weight of the delta peaks at $\pm x_e$, and from it, using (85), we obtain the position of the edge as

$$x_e = \frac{v_0}{\mu \sin(c/2)} g_c(r(x_e^-)). \quad (97)$$

Inside the interval $[-x_e, x_e]$, $r(x)$ is still given by (85), and the densities ρ_s and ρ_d are obtained parametrically using (80) and (81).

The results of this section are compared to numerical simulations for increasing values of N in Fig. 2. The agreement is very good at large N .

F. General case (arbitrary a)

Obtaining an explicit expression for $U(r)$ for general values of a turns out to be more challenging. It is however possible to derive some interesting properties of the stationary density without solving the equations explicitly. In this section κ is of arbitrary sign.

We start by determining the support of the density $[-x_e, x_e]$, assuming that no shocks are present. In the general case, one has for $r > 0$, $U'(r) = -\sqrt{G(U(r))}$ and from the boundary conditions $U(1/2) = 0$. From (43) one sees that $G(0) = v_0^2$ for any parameters, hence $U'(1/2) = -\sqrt{G(0)} = -v_0$ which, using (38), implies that

$$x_e = \frac{v_0 + \kappa}{\mu} \quad (98)$$

for any values of the parameters (as long as there are no shocks). Note that x_e vanishes for $\kappa = -v_0$. This coincides with (92) when $r(x_e^-) = 1/2$, i.e. in the absence of shocks. For $\kappa < -v_0$ the density is a single delta peak at $x = 0$.

1. Presence of shocks

Although in general we do not have an explicit relation between $r(x)$ and x , it is possible to know whether or not shocks are present in the stationary state. Let us recall the general relation (46)

$$\mu x(r) = 2\kappa r - U'(r). \quad (99)$$

Shocks will appear if $x(r)$ is a non-monotonous function of $r \in [-1/2, 1/2]$. Taking the derivative w.r.t. r leads to

$$\mu x'(r) = 2\kappa - U''(r) = 2\kappa - \frac{1}{2}G'(U(r)). \quad (100)$$

Thus shocks are present if there exists a value of $u \in [0, u_0]$ such that $G'(u) = 4\kappa$. Recall that (for $a \neq 1$)

$$G'(u) = -\frac{1}{a} \left(\frac{v_0^2}{u_0} + \frac{b}{a-1} \right) \left(\frac{u}{u_0} \right)^{\frac{1}{a}-1} + \frac{b}{a-1}, \quad (101)$$

where we also recall that $a = \gamma/\mu$ and $b = 4a\kappa$. We have (for $a \neq 1$)

$$G''(u) = -\frac{1}{a^2 u_0} \left((1-a) \frac{v_0^2}{u_0} - b \right) \left(\frac{u}{u_0} \right)^{\frac{1}{a}-2}. \quad (102)$$

$G''(u)$ can be positive or negative depending on the parameters, but it always has a constant sign on $[0, u_0]$, and thus $G'(u)$ is monotonous. Additionally

$$G'(u_0) = 4\kappa - \frac{\mu v_0^2}{\gamma u_0} < 4\kappa. \quad (103)$$

Therefore shocks are present if and only if $G'(0) > 4\kappa$. Let us start with the repulsive case. One has

$$G'(0) = \begin{cases} -\frac{b}{1-a} = -4\kappa \frac{\gamma}{\mu - \gamma} < 0 < 4\kappa & \text{for } a < 1, \\ -\infty & \text{for } a > 1. \end{cases} \quad (104)$$

Therefore $G'(u) < 4\kappa$ for all $u \in [0, u_0]$, so that there are never any shocks in the repulsive case.

Let us now turn to the attractive case $\kappa = -\bar{\kappa} < 0$. Shocks are present if and only if $G'(0) > -4\bar{\kappa}$. For $a < 1$, i.e. $\gamma < \mu$, one has

$$G'(0) = -\frac{b}{1-a} = 4\bar{\kappa} \frac{\gamma}{\mu - \gamma} > 0 > -4\bar{\kappa}, \quad (105)$$

so that shocks are always present. The case $a > 1$ is less straightforward, since in this case $G'(0) = \pm\infty$ where the sign depends on the value of the parameters (see (101)). The condition for shocks to be present is that $G'(0) = +\infty$, i.e.

$$u_0 > \frac{a-1}{-b} v_0^2 = u_0^*. \quad (106)$$

Recall that u_0 is the solution of

$$I(u_0) = \frac{1}{2}, \quad I(u_0) = u_0 \int_0^1 \frac{dw}{\sqrt{v_0^2(1-w^{1/a}) + \frac{bu_0}{a-1}(w-w^{1/a})}}, \quad (107)$$

where $I(u_0)$ is an increasing function of u_0 with $I(0) = 0$. Thus $u_0 > u_0^*$ iff $I(u_0^*) < 1/2$. One has

$$I(u_0^*) = \frac{u_0^*}{v_0} \int_0^1 \frac{dw}{\sqrt{1-w}} = 2 \frac{u_0^*}{v_0} = \frac{1}{2} \left(1 - \frac{\mu}{\gamma}\right) \frac{v_0}{\bar{\kappa}}, \quad (108)$$

and thus the condition for the existence of a shock is

$$\frac{\mu}{\gamma} > 1 - \frac{\bar{\kappa}}{v_0}. \quad (109)$$

Hence in the attractive case there is a region without shocks (left part of region I in Fig. 1) and regions with shocks (III and IV). In the absence of shocks, the position of the edge is given by (98). The analysis of the edge behaviour will be performed below, along with the repulsive case. If shocks are present, the equations (45)-(46) are still valid and determine $r(x)$ for $|x| < x_e$. The position of the edge is then determined by Eq. (92), which is valid for any value of a . Combining with (45)-(46) we obtain that $0 < r(x_e^-) < \frac{1}{2}$ is solution of the equation

$$\bar{\kappa} \left(\frac{1}{2} - r(x_e^-) \right) - U'(r(x_e^-)) = v_0. \quad (110)$$

Once this solution is obtained x_e is determined from (92). Note that $r(x_e^-) = 1/2$ is always solution of (110), however when there is another solution $0 < r(x_e^-) < \frac{1}{2}$ the latter is the correct solution. Since $U'(r) < 0$ for $r > 0$ the equation (110) is valid only for $\bar{\kappa} < 2v_0$. The case $\bar{\kappa} \geq 2v_0$ corresponds to the phase where the density is a single delta peak at $x = 0$ (with $r(x_e^-) \rightarrow 0^+$ as $\bar{\kappa} \rightarrow 2v_0^-$). The limit case $r(x_e^-) \rightarrow \frac{1}{2}^-$ corresponds to the disappearance of the shocks.

We have analyzed these equations above for $a = 1/2$ and we will not study here their general solution. As was discussed in the case $a = 1/2$, we find that x_e is larger in the presence of shocks, due to the convexity of the confining potential.

2. Sign of C and the special line $\frac{\mu}{\gamma} = 1 + \frac{\kappa}{v_0}$

As we have already seen in the case $a = 1/2$, and as we will discuss more generally below, the sign of C influences the slope of the density near the edges of the support when there are no shocks.

The sign of C can be obtained from the above considerations. Indeed, for $a \neq 1$, one has, rewriting (47) using $u_0^* = \frac{1-a}{b} v_0^2$,

$$C = v_0^2 u_0^{-1/a} \left(\frac{u_0}{u_0^*} - 1 \right). \quad (111)$$

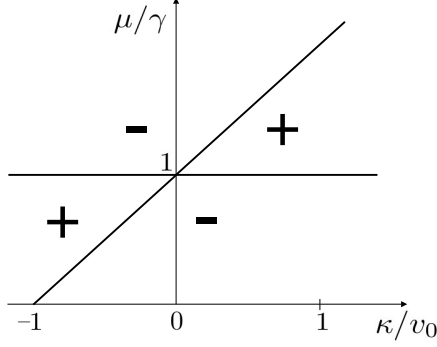


FIG. 5. Sign of the integration constant C . It vanishes on the line $\frac{\mu}{\gamma} = 1 + \frac{\kappa}{v_0}$.

There are 2 cases to distinguish. If $b > 0$ and $a > 1$, or $b < 0$ and $a < 1$, then $u_0^* < 0$, and since $u_0 > 0$ one has $C < 0$. In the opposite case, one has $\text{sgn}(C) = \text{sgn}(u_0 - u_0^*)$, and the computation above shows that $C > 0$ iff the inequality $I(u_0^*) < 1/2$ is satisfied, which is equivalent to (109) for $\kappa = -\bar{\kappa} < 0$ and to $\frac{\mu}{\gamma} < 1 + \frac{\kappa}{v_0}$ for $\kappa > 0$. This is summarized in Fig. 5.

It is possible to determine exactly the shape of the density on the line in the phase diagram where C vanishes. Let us set $C = 0$ in (43), leading to

$$G(u) = \frac{b}{a-1}u + v_0^2. \quad (112)$$

Then (45) becomes

$$\frac{1}{2} - r = \int_0^{U(r)} \frac{du}{\sqrt{\frac{b}{a-1}u + v_0^2}} = \frac{2(a-1)}{b} \left(\sqrt{\frac{b}{a-1}U(r) + v_0^2} - v_0 \right), \quad (113)$$

and thus

$$U(r) = \frac{b}{4(a-1)} \left(\frac{1}{2} - r \right)^2 + v_0 \left(\frac{1}{2} - r \right). \quad (114)$$

The condition $U'(0) = 0$ (see (44)) then implies

$$\frac{b}{4(1-a)} = v_0 \quad \text{i.e.} \quad \frac{\mu}{\gamma} = 1 + \frac{\kappa}{v_0}. \quad (115)$$

This condition defines a line in the phase diagram for which $C = 0$ and which coincide with the one obtained above, see Fig. 5. One can determine the densities on this line. Inserting into (38), this leads to a uniform total density within the support

$$r(x) = \frac{\mu x}{2(\kappa + v_0)} \quad , \quad \rho_s(x) = \frac{\mu}{2(\kappa + v_0)} \quad , \quad \rho_d(x) = \frac{\mu^2 x}{2(\kappa + v_0)^2} \quad , \quad x \in [-x_e, x_e] \quad , \quad x_e = \frac{v_0 + \kappa}{\mu}. \quad (116)$$

where x_e is given by (98). These results coincide with (72) and (73) for $a = 1/2$ and $\kappa = v_0$. Note that there are never shocks along this line.

Finally, C also changes sign on the line $a = 1$, which is more complicated to analyze. We will not consider it here.

3. Edge behaviour (in the absence of shocks)

We now turn to the edge properties of the density. In this section the sign of κ is still arbitrary, but we restrict to the case where there is no shock.

The behaviour of the density near the edges can be obtained by taking the derivative of (36) w.r.t x . This leads to

$$\rho_s(x) = \frac{2\gamma U}{v_0^2 - U'^2} = \frac{2\gamma U}{v_0^2 - G(U)} = \begin{cases} \frac{2\gamma}{\frac{b}{1-a} - CU^{\frac{1}{a}-1}} & \text{for } a \neq 1, \\ -\frac{2\gamma}{b \ln U + C} & \text{for } a = 1. \end{cases} \quad (117)$$

Since $U(1/2) = 0$, there are two cases: for $a \geq 1$, one has $\rho_s(x) \rightarrow 0$ as $x \rightarrow x_e$ and the density vanishes at the edge, while for $a < 1$ the density has a finite limit at the edge

$$\rho_s(x_e) = \frac{2\gamma}{b}(1-a) = \frac{\mu - \gamma}{2\kappa}. \quad (118)$$

More precisely, using $U(r) \simeq v_0(\frac{1}{2} - r) \simeq v_0\rho_s(x_e)(x_e - x)$ near $r = 1/2$, (117) leads to, for $a < 1$, i.e. $\mu/\gamma > 1$,

$$\rho_s(x) \simeq \frac{\mu - \gamma}{2\kappa} \left(1 + C \frac{\mu - \gamma}{4\gamma\kappa} v_0^{\frac{\mu}{\gamma}-1} \left(\frac{1}{2} - r\right)^{\frac{\mu}{\gamma}-1} \right) \simeq \frac{\mu - \gamma}{2\kappa} \left(1 + \frac{C}{2\gamma} \left(\frac{\mu - \gamma}{2\kappa}\right)^{\mu/\gamma} v_0^{\frac{\mu}{\gamma}-1} (x_e - x)^{\frac{\mu}{\gamma}-1} \right). \quad (119)$$

The sign of C was discussed in the previous subsection, see Fig. 5, where we found that whenever $\mu/\gamma < 1 + \kappa/v_0$, one has $C > 0$, which according to (119) means that the density has a local minimum at the edge. If instead $\mu/\gamma > 1 + \kappa/v_0$, then $C < 0$, leading to a local maximum at the edge. Note however that this is only valid for $a < 1$, i.e. $\mu/\gamma > 1$, and in the absence of shocks, i.e. in the repulsive case $\kappa > 0$. This change of edge behaviour marks the difference between the regimes IIa and IIb in Fig. 1.

Let us now determine how $\rho_s(x)$ vanishes at the edge for $a > 1$. Indeed from (117) we find that for x near x_e ,

$$\rho_s(x) \simeq \frac{2\gamma}{|C|} U^{1-\frac{1}{a}}, \quad (120)$$

where we have used that $C < 0$ in this regime. Let us assume that

$$\rho_s(x) \simeq A(x_e - x)^\alpha. \quad (121)$$

Since $U(1/2) = 0$ and $U'(1/2) = -v_0$, see above, this implies

$$U(r) \simeq v_0\left(\frac{1}{2} - r\right) = v_0 \frac{A}{\alpha + 1} (x_e - x)^{\alpha+1}. \quad (122)$$

Plugging into (120) gives

$$A(x_e - x)^\alpha \simeq \frac{2\gamma}{|C|} \left(v_0 \frac{A}{\alpha + 1}\right)^{1-\frac{1}{a}} (x_e - x)^{(\alpha+1)(1-\frac{1}{a})}. \quad (123)$$

This implies $\alpha = a - 1$, and the behavior near the edge, for $a > 1$, i.e. for $\gamma > \mu$, is given by

$$\rho_s(x) \simeq \left(\frac{2\gamma}{|C|}\right)^a \left(\frac{v_0}{a}\right)^{a-1} (x_e - x)^{a-1} = \gamma \left(\frac{2}{|C|}\right)^{\frac{\gamma}{\mu}} (\mu v_0)^{\frac{\gamma}{\mu}-1} (x_e - x)^{\frac{\gamma}{\mu}-1}. \quad (124)$$

This is the same exponent as in the non-interacting case $\kappa = 0$ (with a different amplitude which depends on κ). This is in contrast with the case $\gamma < \mu$, for which the density for $\kappa = 0$ diverges at the edges, while it has a finite limit for $\kappa > 0$.

Finally, in the marginal case $a = 1$, the density again vanishes at the edge but not with an algebraic exponent. One has in this case

$$\rho_s(x) \simeq -\frac{2\gamma}{b \ln U} \simeq -\frac{2\gamma}{b \ln(\frac{1}{2} - r)}. \quad (125)$$

We restrict ourselves to the repulsive case $b > 0$, since in the attractive case there is always a shock for $a = 1$. Using that $\rho_s(x) = r'(x)$ and integrating we obtain

$$-\left(\frac{1}{2} - r\right) \ln\left(\frac{1}{2} - r\right) \simeq \frac{2\gamma}{b}(x_e - x), \quad (126)$$

which implies

$$\frac{1}{2} - r(x) \simeq -\frac{2\gamma}{b} \frac{(x_e - x)}{\ln(x_e - x)} = -\frac{\mu}{2\kappa} \frac{(x_e - x)}{\ln(x_e - x)}. \quad (127)$$

Taking the derivative, we obtain at leading order the density near the edge

$$\rho_s(x) \simeq \frac{\mu}{2\kappa} \frac{1}{(\ln(x_e - x))^2}. \quad (128)$$

It is worth noting that this inverse logarithmic divergence only occurs for $\kappa > 0$ (in the non-interacting case the density is uniform on $x \in [-v_0/\mu, v_0/\mu]$ for $a = 1$, i.e. $\gamma = \mu$).

Edge behaviour of $\rho_{\pm}(x)$. Finally, let us briefly consider the densities of $+$ and $-$ particles independently. For x near x_e , one has

$$\rho_d(x) = -\frac{1}{v_0} \partial_x U(r(x)) \simeq -\frac{1}{v_0} \partial_x [v_0(\frac{1}{2} - r)] = \rho_s(x). \quad (129)$$

Hence $\rho_+(x) \simeq \rho_s(x)$, while $\rho_-(x)$ vanishes at the edge with a larger exponent. In the case $\kappa = 0$, $\rho_-(x)$ vanishes with an exponent $\frac{\gamma}{\mu}$ near x_e . In general we have

$$\rho_-(x) = \frac{1}{2}(\rho_s(x) - \rho_d(x)) = \frac{1}{2}\left(1 + \frac{U'(r)}{v_0}\right)\rho_s(x). \quad (130)$$

For $a < 1$, one has from (53) $U''(1/2) = \frac{1}{2}G'(0) = \frac{b}{2(a-1)}$, and thus near x_e ,

$$U'(r) \simeq -v_0 + \frac{b}{2(1-a)}\left(\frac{1}{2} - r\right) \simeq -v_0 + \frac{b}{2(1-a)} \frac{\mu - \gamma}{2\kappa}(x_e - x) \simeq -v_0 + \gamma(x_e - x). \quad (131)$$

Inserting in (130) we obtain, for $\gamma < \mu$,

$$\rho_-(x) \simeq \frac{1}{2} \frac{\gamma}{v_0}(x_e - x)\rho_s(x) \simeq \frac{\gamma(\mu - \gamma)}{4\kappa v_0}(x_e - x). \quad (132)$$

In the case $a > 1$, i.e. $\gamma > \mu$, one has instead

$$U'(r) = -\sqrt{G(U(r))} \simeq -v_0\left(1 + \frac{C}{2v_0^2}U(r)^{1/a}\right). \quad (133)$$

Combining with (122), (124) and (130) one obtains,

$$\rho_-(x) \simeq \frac{|C|}{4v_0^2}U(r)^{1/a}\rho_s(x) \simeq \frac{\mu}{2v_0}(x_e - x)\rho_s(x) \simeq \frac{\gamma}{2}\left(\frac{2\mu}{|C|}\right)^{\frac{\gamma}{\mu}}v_0^{\frac{\gamma}{\mu}-2}(x_e - x)^{\gamma/\mu}. \quad (134)$$

Similarly for $a = 1$, i.e. $\gamma = \mu$, one obtains

$$\rho_-(x) \simeq -\frac{b}{4v_0^2} U(r) \ln U(r) \rho_s(x) \simeq \frac{\mu^2}{4v_0\kappa} \frac{x_e - x}{(\ln(x_e - x))^2}, \quad (135)$$

where once again (as in (128)) the logarithmic behaviour is a special feature of the interacting case $\kappa > 0$ (since it vanishes linearly when $\kappa = 0$).

For $\gamma > \mu$, the exponent is again the same as in the $\kappa = 0$ case. In general, we observe a difference of 1 in the exponent between $\rho_+(x)$ and $\rho_-(x)$, as in the non-interacting [12] and the active DBM cases [48].

G. Phase diagram

The results of this section are summarized in Fig. 1, which shows a diagram of the different regimes for the stationary density. These results are confirmed by numerical simulations, where we solve numerically the stochastic equation of motion for N RTP's (with N up to 10^3) and measure the stationary densities by averaging over a large time window. We find that there are 5 phases in total:

- Phase I: A smooth phase which exists both in the repulsive ($\mu/\gamma < 1$) and in the attractive case ($\mu/\gamma < 1 - \bar{\kappa}/v_0$), in which the density vanishes at the edges with an exponent $\frac{\gamma}{\mu} - 1$ identical to the exponent of the non-interacting case.
- Phase IIa: A strongly repulsive phase ($1 < \mu/\gamma < 1 + \kappa/v_0$), in which the density has a discontinuity at the edges, but is minimal at the edges.
- Phase IIb: A strongly active phase ($\mu/\gamma > 1 + \kappa/v_0$), in which the density has a discontinuity at the edges and is maximal at the edges.
- Phase III: A strongly attractive phase ($\mu/\gamma > 1 - \bar{\kappa}/v_0$ and $\bar{\kappa}/v_0 < 2$), in which the density has delta peaks at the edges. We find in our numerical simulations with $N = 1000$ that the density is maximal at the edges (independently of the sign of C).
- Phase IV: A condensed phase ($\bar{\kappa}/v_0 > 2$), in which the density is a delta peak at $x = 0$.

The passage from phase IIa to IIb is only a crossover since it also occurs at finite N (see Fig. 1), while the other phases have distinct features which only occur for $N \rightarrow +\infty$. At finite N , we find from our numerical simulations that both the jumps at the edge of the density in phases IIa and IIb and the shocks in phase III have a small width which decays to zero as N increases, see Fig 2. In the case of the shocks, this broadening is due to fluctuations in the number of particles contained in the clusters of particles located at the edge, which lead to fluctuations in their position. The phase IV is special: if at finite N we measure the density in the reference frame of the center of mass, it will always be a delta peak for $\kappa \leq -2v_0$ for any $N \geq 2$. The absolute total density however remains smooth at finite N since the center of mass reaches a non trivial stationary distribution.

H. Limit of small γ and fixed points

For $\gamma \ll \mu$, the stationary density is closely related to the fixed points of the dynamics at fixed σ_i 's, given by the roots of the set of equations

$$V'(x_i) = \mu x_i = \frac{\kappa}{N} \sum_{j=1}^N \text{sgn}(x_i - x_j) + v_0 \sigma_i \quad , \quad i = 1, \dots, N. \quad (136)$$

In the limit $\gamma/\mu \rightarrow 0$ the system spends most of its time near these fixed points before the $\sigma_i(t)$ switch to another value. In the stationary state each set of σ_i is equiprobable. At finite N , since these fixed points

are reached in finite time, they appear as sharp peaks in the density (which become delta peaks for $\gamma = 0^+$), see Figure 6. A similar discussion was detailed in the case of the active DBM in [48].

The attractive case is quite straightforward to analyze: in the limit $\gamma \rightarrow 0^+$, the particles will form two clusters at positions $\pm x_e$ containing respectively all the + and - particles. Each clusters thus contains $N/2$ particles. The position x_e is simply given by the balance of forces

$$\mu x_e = v_0 - \frac{\bar{\kappa}}{2}. \quad (137)$$

which is larger than the position of the edge in the absence of shocks $\mu x_e = v_0 - \bar{\kappa}$, see (98). For $\bar{\kappa} \geq 2v_0$, the two clusters merge and $x_e = 0$.

The repulsive case is more involved. For $v_0 = 0$, denoting $x_i^0 = \frac{\kappa}{2N\mu}(N+1-2i)$, there are $N!$ fixed points, which take the form $x_i = x_{\tau(i)}^0$ where τ is any permutation of the particles. The particles are thus regularly spaced with separation $\frac{2\kappa}{N\mu}$. For $v_0 < \frac{\kappa}{N}$ each fixed point is simply shifted as $x_i = x_{\tau(i)}^0 + \frac{v_0}{\mu}\sigma_i$. As v_0 increases beyond $\frac{\kappa}{N}$, a natural conjecture is that there is a transition to a set of $N_+!N_-!$ fixed points where all the + particles are to the right of all the - particles (which are identical up to permutations in each group). The positions are still given by $x_i = x_{\tau(i)}^0 + \frac{v_0}{\mu}\sigma_i$ but now the permutation $\tau \in S_{N_+} \times S_{N_-}$ only permutes member of each group.

In the limit $N \rightarrow +\infty$, the fraction of + and - particles are the same and thus all + particles are evenly spaced on $[\frac{v_0}{\mu}, \frac{v_0+\kappa}{\mu}]$ and all - particles are evenly spaced on $[-\frac{v_0+\kappa}{\mu}, -\frac{v_0}{\mu}]$. Thus the density in the double limit $N \rightarrow +\infty, \gamma \rightarrow 0$, is

$$\rho_s(x) = \frac{\mu}{2\kappa} \quad \text{for} \quad \frac{v_0}{\mu} < |x| < \frac{v_0 + \kappa}{\mu}. \quad (138)$$

Note that this regime $\gamma/\mu \ll 1$ is a limit of the phase IIb in Fig. 1.

This result can also be derived by solving (31) for $\gamma = 0$, and generalized to a larger class of potentials $V(x)$. Indeed the first equation in (31) leads to $s'(x) = \frac{V'(x) - 2\kappa r(x)}{v_0} r'(x)$. Inserting in the second equation gives

$$v_0^2 r'(x) = (V'(x) - 2\kappa r(x))^2 r'(x), \quad (139)$$

i.e. $r'(x) = s'(x) = 0$ or

$$r(x) = \frac{V'(x) \pm v_0}{2\kappa}, \quad s'(x) = \mp r'(x). \quad (140)$$

The second equation means that the + and - particles are separated. Let us assume for simplicity $V(x)$ to be convex, twice differentiable with $V'(\pm\infty) = \pm\infty$. In that case one can define x_0^\pm and x_e^\pm as the roots of

$$V'(x_0^\pm) = \pm v_0, \quad V'(x_e^\pm) = \pm(v_0 + \kappa). \quad (141)$$

The support of the density has two components, with

$$r(x) = \begin{cases} \frac{V'(x) - v_0}{2\kappa} & , \quad x \in [x_0^+, x_e^+] , \\ \frac{V'(x) + v_0}{2\kappa} & , \quad x \in [x_e^-, x_0^-] , \end{cases} \quad (142)$$

where $\rho_s(x) = \frac{V''(x)}{2\kappa}$ in each component, and $\rho_d(x) = \rho_s(x)$ for $x \in [x_0^+, x_e^+]$ and $\rho_d(x) = -\rho_s(x)$ for $x \in [x_e^-, x_0^-]$. Taking $V(x) = \frac{\mu}{2}x^2$, this is compatible with (138).

We have tested these predictions in a numerical simulation of the stationary density for various values of N , for $\gamma \ll \mu$, see Fig. 6. For low values of N the density is well approximated by a sum of delta peaks corresponding to the fixed points. One sees that some of these peaks disappear as v_0 is increased, as predicted. For large values of N the density become smooth. As $\gamma \rightarrow 0$ a gap region develops where the density vanishes, with two uniform square densities on each side, for each \pm species respectively.

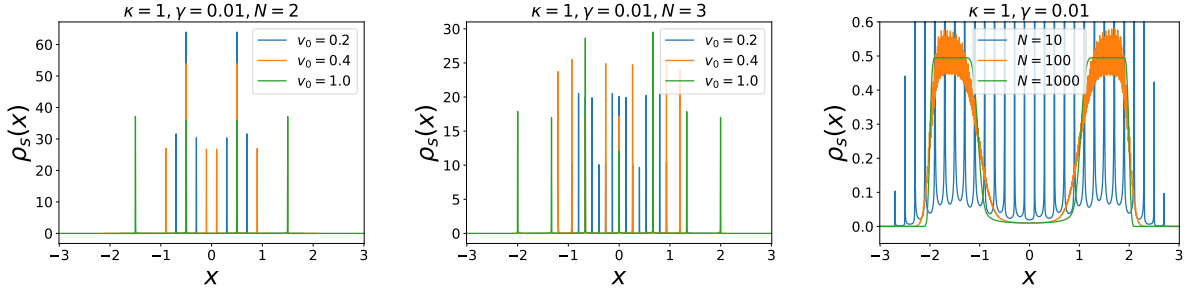


FIG. 6. Plots of the stationary density $\rho_s(x)$ in the repulsive case with $\kappa = 1$, $\mu = 1$ and $\gamma = 0.01$. Left and central panels: plots for $N = 2$ and 3 with different values of v_0 . The density is mostly composed of delta peaks corresponding to the different fixed points of the system. The delta peaks closest to the center disappear for $v_0 > \kappa/N$ (e.g. we go from 6 to 4 peaks for $N = 2$). Right: Plots for $v_0 = 1$ and increasing values of N . As $N \rightarrow +\infty$, $\rho_s(x)$ converges to a smooth density on $[-\frac{v_0+\kappa}{\mu}, \frac{v_0+\kappa}{\mu}]$. In the limit $\gamma \rightarrow 0$, this density is uniform on $[-\frac{v_0+\kappa}{\mu}, -\frac{v_0}{\mu}] \cup [\frac{v_0}{\mu}, \frac{v_0+\kappa}{\mu}]$ and zero on $[-\frac{v_0}{\mu}, \frac{v_0}{\mu}]$.

IV. NON-RECIPROCAL ACTIVE RANK DIFFUSIONS IN A LINEAR POTENTIAL

A. Equation for the rank fields for a general non-reciprocal interaction

We now consider a more general set of stochastic equation of motion, where the interaction potential between particles i and j still depends on their rank, but also on their states $\sigma_i(t)$ and $\sigma_j(t)$, with interaction strength $\kappa_{\sigma_i(t), \sigma_j(t)}$, where the $\kappa_{\pm, \pm}$ are a given set of four parameters

$$\frac{dx_i}{dt} = \sum_{j=1}^N \frac{\kappa_{\sigma_i(t), \sigma_j(t)}}{N} \text{sgn}(x_i - x_j) - V'_{\sigma_i(t)}(x_i) + v_0 \sigma_i(t) + \sqrt{2T} \xi_i(t). \quad (143)$$

Here $\kappa_{\sigma, \sigma'}$ parameterizes the force exerted by a particle in state σ' on a particle in state σ . We do not assume here that the matrix $\kappa_{\sigma, \sigma'}$ is symmetric.

In this case the Dean-Kawasaki equations become

$$\begin{aligned} \partial_t \rho_\sigma(x, t) &= T \partial_x^2 \rho_\sigma(x, t) + \partial_x [\rho_\sigma(x, t) (-v_0 \sigma + V'_\sigma(x) - \sum_{\sigma'} \kappa_{\sigma, \sigma'} \int dy \rho_{\sigma'}(y, t) \text{sgn}(x - y))] \\ &+ \gamma \rho_{-\sigma}(x, t) - \gamma \rho_\sigma(x, t) + O\left(\frac{1}{\sqrt{N}}\right). \end{aligned} \quad (144)$$

We define

$$h_\pm(x) = \frac{1}{2} (r(x) \pm s(x)) = \int_{-\infty}^x dy \rho_\pm(y, t) - \frac{1}{4}, \quad (145)$$

where $r(x)$ and $s(x)$ are defined as in (28), such that

$$\rho_\pm = \frac{1}{2} (\rho_s \pm \rho_d) = \partial_x \frac{r \pm s}{2} = \partial_x h_\pm, \quad (146)$$

and we rewrite the interaction term using

$$\begin{aligned}
\int dy \rho_{\pm}(y, t) \text{sgn}(x - y) &= \int dy \partial_y \left(\frac{r(y, t) \pm s(y, t)}{2} \right) \text{sgn}(x - y) \\
&= r(x, t) \pm s(x, t) + \left[\left(\frac{r(y, t) \pm s(y, t)}{2} \right) \text{sgn}(x - y) \right]_{-\infty}^{+\infty} \\
&= r(x, t) \pm s(x, t) - \frac{1}{2} (r(-\infty, t) + r(+\infty, t)) - \frac{1}{2} (s(-\infty, t) + s(+\infty, t)) \\
&= r(x, t) \pm s(x, t) - \frac{1}{2} \int_{-\infty}^{+\infty} dy \rho_d(y, t) \\
&= r(x, t) \pm s(x, t) - \frac{1}{2} (p_+(t) - p_-(t)) .
\end{aligned} \tag{147}$$

For simplicity for now we will assume that we start from $p_+(t=0) = p_-(t=0) = 1/2$ and neglect again the noise at large N so that $p_+(t) = p_-(t) = 1/2$ at all times. Hence we obtain at large N

$$\partial_t \rho_{\sigma}(x, t) = T \partial_x^2 \rho_{\sigma}(x, t) + \partial_x [\rho_{\sigma}(x, t) (-v_0 \sigma + V'_{\sigma}(x) - 2 \sum_{\sigma'} \kappa_{\sigma, \sigma'} h_{\sigma'}(x, t))] + \gamma \rho_{-\sigma}(x, t) - \gamma \rho_{\sigma}(x, t) , \tag{148}$$

where because of our assumptions ($p_+(t) = p_-(t) = 1/2$) one has the boundary conditions $h_{\sigma}(\pm\infty, t) = \pm 1/4$. We can thus integrate the equation and obtain

$$\partial_t h_{\sigma}(x, t) = T \partial_x^2 h_{\sigma}(x, t) + (-v_0 \sigma + V'_{\sigma}(x) - 2 \sum_{\sigma'} \kappa_{\sigma, \sigma'} h_{\sigma'}(x, t)) \partial_x h_{\sigma}(x, t) + \gamma h_{-\sigma}(x, t) - \gamma h_{\sigma}(x, t) . \tag{149}$$

B. A simple example of non-reciprocal interaction

Let us consider a non-reciprocal interaction of the form

$$\kappa_{+-} = -\kappa_{-+} = -b \quad , \quad \kappa_{++} = \kappa_{--} = 0 . \tag{150}$$

This means that, if $b > 0$, $+$ particles are attracted to $-$ particles, while $-$ particles are repulsed by $+$ particles, both with a force of norm b/N independent of the distance. Note that there is a symmetry ($b \rightarrow -b$, $x \rightarrow -x$, $h_+ \leftrightarrow h_-$). We thus restrict our study to $b > 0$, since the case $b < 0$ can be obtained by symmetry. We look for the stationary measure at $T = 0$, in presence of a linear external potential $V'(x) = a \text{sgn}(x)$ (with $a > 0$, since in the absence of external potential there is no stationary state and the particles escape to infinity). The stationary equations read

$$0 = (-v_0 + a \text{sgn}(x) + 2bh_-) h'_+ + \gamma h_- - \gamma h_+ , \tag{151}$$

$$0 = (v_0 + a \text{sgn}(x) - 2bh_+) h'_- + \gamma h_+ - \gamma h_- . \tag{152}$$

This leads to, taking the sum and difference,

$$0 = -v_0 s' + a \text{sgn}(x) r' + 2b(h_- h'_+ - h_+ h'_-) , \tag{153}$$

$$0 = -v_0 r' + a \text{sgn}(x) s' + 2b(h_+ h_-)' - 2\gamma s , \tag{154}$$

which can be rewritten as

$$0 = -v_0 s' + a \text{sgn}(x) r' + b r s' - b s r' , \tag{155}$$

$$0 = -v_0 r' + a \text{sgn}(x) s' + b r r' - b s s' - 2\gamma s . \tag{156}$$

The first equation can be rewritten as

$$(v_0 - br) \frac{ds}{dr} = (\pm a - bs) , \tag{157}$$

where $\pm a = a \operatorname{sgn}(x)$. It integrates into

$$s = \pm \frac{a}{b} + (br - v_0)c_{\pm} . \quad (158)$$

We assume for now that there are no shocks outside of $x = 0$. In this case, the constant c_{\pm} is determined by the constraints $s(\pm\infty) = 0$ and $r(\pm\infty) = \pm 1/2$. One finds

$$c_+ = \frac{2a}{b(2v_0 - b)} \quad , \quad c_- = -\frac{2a}{b(2v_0 + b)} , \quad (159)$$

which leads to

$$s = \begin{cases} a \frac{1 - 2r}{b - 2v_0} & \text{for } x > 0 , \\ -a \frac{1 + 2r}{b + 2v_0} & \text{for } x < 0 . \end{cases} \quad (160)$$

Going back to Eq. (156) and inserting (160), we find, for $x > 0$,

$$\frac{((2v_0 - b)^2 - 4a^2)(v_0 - br(x))}{(2v_0 - b)^2} r'(x) = \frac{2a\gamma(1 - 2r(x))}{2v_0 - b} , \quad (161)$$

that is

$$\frac{v_0 - br}{1 - 2r} dr = \frac{2a\gamma(2v_0 - b)}{(2v_0 - b)^2 - 4a^2} dx , \quad (162)$$

which integrates into

$$b(1 - 2r) + (2v_0 - b) \log(1 - 2r) = -\frac{8a\gamma(2v_0 - b)}{(2v_0 - b)^2 - 4a^2} x + C_+ , \quad (163)$$

where C_+ is a constant that remains to be determined.

The solution, assuming that it exists, decays exponentially at large x and can be written as

$$1 - 2r(x) = \frac{2v_0 - b}{b} W \left(\frac{b}{2v_0 - b} e^{-A_+ x + \frac{C_+}{2v_0 - b}} \right) , \quad A_+ = \frac{8a\gamma}{(2v_0 - b)^2 - 4a^2} , \quad (164)$$

where W is the main branch of the Lambert function, which is the real (and largest) root of

$$W(z)e^{W(z)} = z , \quad (165)$$

for $z \in [-1/e, +\infty[$, with $W(z) \simeq z$ for z near $z = 0$. Thus the density decays as $\rho_s(x) \sim e^{-A_+ x}$ for $x \rightarrow +\infty$.

For $x < 0$ one finds by a similar calculation

$$\frac{((2v_0 + b)^2 - 4a^2)(v_0 - br(x))}{(2v_0 + b)^2} r'(x) = \frac{2a\gamma(1 + 2r(x))}{2v_0 + b} , \quad (166)$$

that is

$$\frac{v_0 - br}{1 + 2r} dr = \frac{2a\gamma(2v_0 + b)}{(2v_0 + b)^2 - 4a^2} dx , \quad (167)$$

which integrates into

$$b(1 + 2r) - (2v_0 + b) \log(1 + 2r) = -\frac{8a\gamma(2v_0 + b)}{(2v_0 + b)^2 - 4a^2}x + C_- , \quad (168)$$

where C_- is another constant to be determined.

Assuming again that a solution exists, it reads

$$1 + 2r(x) = -\frac{2v_0 + b}{b}W\left(-\frac{b}{2v_0 + b}e^{A_-x - \frac{C_-}{2v_0 + b}}\right) , \quad A_- = \frac{8a\gamma}{(2v_0 + b)^2 - 4a^2} . \quad (169)$$

Thus the density decays as $\rho_s(x) \sim e^{A_-x}$ for $x \rightarrow -\infty$.

We see that A_+ and A_- are the characteristic inverse length-scale of the N particle bound state on the right and left side of $x = 0$ respectively. As $a \rightarrow 0$ the size of the bound state thus diverges as $\sim 1/a$, consistent with the absence of a stationary state for $a = 0$.

We have thus determined the full solution for the density of particles $\rho_s(x) = \partial_x r(x)$, up to two integration constants C_+ and C_- . We thus need two additional boundary conditions. As we will see below, the choice of these boundary conditions is highly non-trivial and depends on the parameters, leading to different regimes. In particular, the constants A_{\pm} should be positive so that the density correctly decays at infinity. The condition $A_+ > 0$ requires that $a < |v_0 - b/2|$. If this condition is not satisfied, the density is restricted to the interval $(-\infty, 0]$ and a shock appears at $x = 0$. Similarly, $A_- > 0$ requires that $a < v_0 + b/2$. For $a > v_0 + b/2$, the density will thus be a single delta peak at $x = 0$ (phase IV in Fig. 3), which was to be expected since in this case since the noise and the interaction are not strong enough to compete with the confining potential.

One way to check if a solution is consistent is to consider the total force on a particle at a given position. In particular, to know if a cluster is present at $x = 0$ and if the particles can access the regions $x > 0$ and $x < 0$, one should compute the force at $x = 0^-$, $x = 0^+$ and exactly at $x = 0$. Let us denote $f_{\pm}(x)$ the total force on a \pm particle at position x and let us write its expression near $x = 0$ as a function of the rank fields $h_{\pm}(x) = \int_{-\infty}^x \rho_{\pm}(y)dy - \frac{1}{4}$. For a $+$ particle it reads

$$\begin{aligned} f_+(0^+) &= v_0 - a - b \int_{-\infty}^{0^+} \rho_-(y)dy + b \int_{0^+}^{+\infty} \rho_-(y)dy = v_0 - a - 2bh_-(0^+) , \\ f_+(0) &= v_0 - b \int_{-\infty}^{0^-} \rho_-(y)dy + b \int_{0^+}^{+\infty} \rho_-(y)dy = v_0 - b(h_-(0^+) + h_-(0^-)) , \\ f_+(0^-) &= v_0 + a - b \int_{-\infty}^{0^+} \rho_-(y)dy + b \int_{0^+}^{+\infty} \rho_-(y)dy = v_0 + a - 2bh_-(0^-) , \end{aligned} \quad (170)$$

and similarly for a $-$ particle,

$$\begin{aligned} f_-(0^+) &= -v_0 - a + 2bh_+(0^+) , \\ f_-(0) &= -v_0 + b(h_+(0^+) + h_+(0^-)) , \\ f_-(0^-) &= -v_0 + a + 2bh_+(0^-) . \end{aligned} \quad (171)$$

A cluster of $+$ particles forms at $x = 0$ if either $f_+(0) < 0$ and $f_+(0^-) > 0$, or if $f_+(0) > 0$ and $f_+(0^+) < 0$ (and similarly for $-$ particles). Another sufficient condition is of course $f_{\pm}(0^-) > 0$ and $f_{\pm}(0^+) < 0$. In addition, the density vanishes on the half line $x > 0$ iff $(f_+(0) < 0$ or $f_+(0^+) < 0)$ and $(f_-(0) < 0$ or $f_-(0^+) < 0)$ (and symmetrically for $x < 0$). One can see that, when $a > v_0 + b/2$, since $|h_{\pm}(x)| < 1/4$, one necessarily has $f_{\pm}(0^+) < 0$ and $f_{\pm}(0^-) > 0$, and thus all the particles remain at $x = 0$ (phase IV). Of course, in general the forces $f_{\pm}(x)$ can only be computed a posteriori from the rank fields, but we will use them to check the consistency of our solutions.

Below we will consider in order the 3 non-trivial phases of Fig. 3: phase I, for $a < v_0 - b/2$, where there is no shock, phase II, for $|v_0 - b/2| < a < v_0 + b/2$, where there is a shock at $x = 0$ and the density is restricted to $(-\infty, 0]$, and phase III, for $a < b/2 - v_0$, where there is a shock at $x = 0$ but the density is again supported on the whole real axis.

1. Phase I: Absence of shock

Let us first assume that there is no shock, i.e. that $r(x)$ and $s(x)$ are continuous at $x = 0$. Using Eq. (160), this leads to the condition

$$r(0) = \frac{b}{4v_0} \quad , \quad s(0) = -\frac{a}{2v_0} . \quad (172)$$

The fraction of particles on the negative side is $r(0) + \frac{1}{2} = \frac{1}{2} + \frac{b}{4v_0}$. Hence for $b > 0$ there are more particles on the negative part of the real axis. Note that (172) implies that

$$h_+(0) = \frac{r(0) + s(0)}{2} = \frac{b - 2a}{8v_0} \quad , \quad h_-(0) = \frac{r(0) - s(0)}{2} = \frac{b + 2a}{8v_0} , \quad (173)$$

and remember that each field varies in $[-1/4, 1/4]$. In particular, the condition $h_-(0) < 1/4$ implies the following condition for the absence of shocks:

$$a < v_0 - b/2 . \quad (174)$$

Note that since $a > 0$, one must also have $b < 2v_0$. The other bounds on $h_{\pm}(0)$ imply $a < v_0 + b/2$, which is less restrictive for $b > 0$, and $a > b/2 - v_0$ which also always holds for $a > 0$ and $b < 2v_0$. As we will see below, when the condition (174) is violated, a shock appears at $x = 0$. From the expression of $h_-(0)$, we expect that all the $-$ particles will be on the left in this regime, since $h_-(0) \rightarrow 1/4$ as $a \rightarrow v_0 - b/2$.

As mentioned above, let us also compute the total force near $x = 0$. One has, using that $a < v_0 - b/2$

$$\begin{aligned} f_+(0^+) &= v_0 - a - \frac{b}{4v_0}(b + 2a) > 0 , & f_-(0^+) &= -v_0 - a + \frac{b}{4v_0}(b - 2a) < 0 , \\ f_+(0) &= v_0 - \frac{b}{4v_0}(b + 2a) > 0 , & f_-(0) &= -v_0 + \frac{b}{4v_0}(b - 2a) < 0 , \\ f_+(0^-) &= v_0 + a - \frac{b}{4v_0}(b + 2a) > 0 , & f_-(0^-) &= -v_0 + a + \frac{b}{4v_0}(b - 2a) < 0 . \end{aligned} \quad (175)$$

Thus, close to $x = 0$, the $+$ particles all move towards the right and the $-$ particles all move towards the left, consistent with our hypotheses that there is no shock at $x = 0$ and that the particles have access to the whole real axis.

Evaluating (163) at $x = 0$ and using (172) we find that in the absence of shock at $x = 0$,

$$C_+ = (2v_0 - b) \left(\frac{b}{2v_0} + \log\left(1 - \frac{b}{2v_0}\right) \right) . \quad (176)$$

Similarly, evaluating (168) at $x = 0$ and using (172) we obtain,

$$C_- = (2v_0 + b) \left(\frac{b}{2v_0} - \log\left(1 + \frac{b}{2v_0}\right) \right) . \quad (177)$$

Inserting into (164) and (169), we obtain the full solution in the regime where $0 < b < 2v_0$ and $2a < 2v_0 - b$,

$$1 - 2r(x) = \frac{2v_0 - b}{b} W \left(\frac{b}{2v_0} e^{-A_+ x + \frac{b}{2v_0}} \right) , \quad A_+ = \frac{8a\gamma}{(2v_0 - b)^2 - 4a^2} , \quad \text{for } x > 0 , \quad (178)$$

$$1 + 2r(x) = -\frac{2v_0 + b}{b} W \left(-\frac{b}{2v_0} e^{A_- x - \frac{b}{2v_0}} \right) , \quad A_- = \frac{8a\gamma}{(2v_0 + b)^2 - 4a^2} , \quad \text{for } x < 0 . \quad (179)$$

By construction one has $W\left(\frac{b}{2v_0}e^{\frac{b}{2v_0}}\right) = \frac{b}{2v_0}$ which yields $r(0) = \frac{b}{4v_0}$ as required. Note that the lower edge $z = -1/e$ of the first branch of the Lambert function $W(z)$ is only reached as $b \rightarrow 2v_0$.

The total density is obtained by taking a derivative with respect to x , leading to,

$$\rho_s(x) = A_+ \frac{2v_0 - b}{2b} \left(1 - \frac{1}{1 + W\left(\frac{b}{2v_0}e^{-A_+x + \frac{b}{2v_0}}\right)} \right), \quad \text{for } x > 0, \quad (180)$$

$$\rho_s(x) = A_- \frac{2v_0 + b}{2b} \left(\frac{1}{1 + W\left(-\frac{b}{2v_0}e^{A_-x - \frac{b}{2v_0}}\right)} - 1 \right), \quad \text{for } x < 0, \quad (181)$$

where we have used that $W'(z) = \frac{W(z)}{z(1+W(z))}$. One finds

$$\rho_s(0^+) = \frac{B_+}{2} \frac{2v_0 - b}{2v_0 + b}, \quad \rho_s(0^-) = \frac{B_-}{2} \frac{2v_0 + b}{2v_0 - b}. \quad (182)$$

The ratio

$$\frac{\rho_s(0^-)}{\rho_s(0^+)} = \frac{(2v_0 + b)^2 (2v_0 - b)^2 - 4a^2}{(2v_0 - b)^2 (2v_0 + b)^2 - 4a^2} = \frac{1 - \frac{4a^2}{(2v_0 - b)^2}}{1 - \frac{4a^2}{(2v_0 + b)^2}} \quad (183)$$

is smaller than unity for $b > 0$. On the other hand the decay is slower on the negative side for $b > 0$, since then $A_- < A_+$. As we have already noted above, the fact that $r(0) > 0$ means that this second effect dominates and that there are more particles on the negative side than on the positive side.

2. Phase II: Shock at $x = 0$ and no particles for $x > 0$

Considering the solution (178)-(179), we noticed above that two things happen as $a \rightarrow (v_0 - b/2)^-$. First, A_+ diverges, suggesting that the density vanishes on the positive side of the real axis. Second, $h_-(0) \rightarrow 1/4$, suggesting that all $-$ particles are located at $x < 0$. However, $h_+(0)$ does not converge to $1/4$ in that limit (it converges to $\frac{1}{4} - \frac{a}{2v_0}$), which suggests the existence of a cluster (i.e. a delta peak) of $+$ particles at $x = 0$ for $a > v_0 - b/2$ (of weight $a/(2v_0)$ on the frontier between phase I and II).

Let us thus look for a solution in the regime $a > v_0 - b/2$, assuming that the density vanishes for $x > 0$ (thus $h_+(0^+) = h_-(0^+) = 1/4$). In this case we only need to determine the constant C_- and the weight of the delta peak at $x = 0$. In addition, let us assume that $h_-(0^-) = 1/4$ remains frozen, meaning that there are no $-$ particles in the shock at $x = 0$. Using Eq. (160), which remains valid as long as there is no shock outside of $x = 0$, we obtain

$$h_+(0^-) = \frac{1}{4} - \frac{2a}{b + 2v_0 + 2a}, \quad (184)$$

and thus,

$$r(0^-) = \frac{b + 2v_0 - 2a}{2(b + 2v_0 + 2a)} = \frac{1}{2} - \frac{2a}{b + 2v_0 + 2a}, \quad s(0^-) = -\frac{2a}{b + 2v_0 + 2a}. \quad (185)$$

Note that $h_+(0^-) \rightarrow -1/4$ as $a \rightarrow v_0 + b/2$, consistent with the fact that all particles remain at $x = 0$ for $a > v_0 + b/2$, i.e. in Phase IV. Note also that $h_+(0^-) \rightarrow 1/4 - a/(2v_0)$ as $a \rightarrow v_0 - b/2$ (for $b < 2v_0$), meaning that the weight of the delta peak does not vanish continuously as one approaches this line (i.e. the boundary between the phases I and II).

Once again, let us compute the total force near $x = 0$. One has,

$$\begin{aligned}
f_+(0^+) &= v_0 - a - \frac{b}{2}, & f_-(0^+) &= -v_0 - a + \frac{b}{2}, \\
f_+(0) &= v_0 - \frac{b}{2}, & f_-(0) &= -v_0 + \frac{b}{2} - \frac{2ab}{b + 2v_0 + 2a}, \\
f_+(0^-) &= v_0 + a - \frac{b}{2}, & f_-(0^-) &= -v_0 + a + \frac{b}{2} - \frac{4ab}{b + 2v_0 + 2a}.
\end{aligned} \tag{186}$$

Let us study the sign of these forces in detail. First, as long as the condition $a > |v_0 - b/2|$ is satisfied, one has $f_+(0^+) < 0$ and $f_+(0^-) > 0$, implying that a cluster of + particles is indeed present at $x = 0$. In addition, in this region one has $f_-(0^+) < 0$. Thus, no particle can access the region $x > 0$, in agreement with our assumptions. In fact, as long as $-v_0 + b/2 < a < v_0 + b/2$, $f_-(x)$ is strictly negative in the whole vicinity of $x = 0$, which means that for $|v_0 - b/2| < a < v_0 + b/2$ all the - particles remain in the region $x < 0$ (and do not contribute to the cluster at $x = 0$), as we have assumed. Of course, since the - particles can turn into + particles, this implies that some + particles will also be present in this region. However, once they have reached $x = 0$ they remain there until they switch sign again.

The sign of the forces $f_{\pm}(x)$ in the vicinity of $x = 0$ is thus compatible with the assumptions of this section (no particles for $x > 0$ and no - particles at $x = 0$) in the region $|v_0 - b/2| < a < v_0 + b/2$, which defines phase II and which is also the region where $A_- > 0$ and $A_+ < 0$. Let us discuss the limits to the phases IV, I and III respectively. For $a > v_0 + b/2$, i.e. phase IV, one has $f_-(0^-) < 0$ and all the particles remain at $x = 0$. For $b < 2v_0$ and $a < v_0 - b/2$, i.e. phase I, one finds that $f_+(0^+) > 0$ and $f_+(0) > 0$. Thus the + particles do not remain confined at $x = 0$ and can access the region $x > 0$. This means that the correct solution in this region is indeed the one obtained in the previous section, in the absence of shocks. Finally, and perhaps more surprisingly, for $b > 2v_0$ and $a < -v_0 + b/2$, i.e. in phase III, one finds that $f_+(x)$ is strictly negative and $f_-(x)$ is strictly positive in the whole vicinity of $x = 0$, implying that the particles have again access to the whole real axis. In this case, the present assumptions are thus incorrect. This last case will be studied in the next section.

We now determine the full solution for the density in the region $|v_0 - b/2| < a < v_0 + b/2$, where the present assumptions are valid. Eq. (168) remains true even with a shock at $x = 0$, but now the constant C_- is determined by (190). This gives

$$C_- = (b + 2v_0) \left(\frac{2b}{2a + b + 2v_0} - \log \left(\frac{2(b + 2v_0)}{2a + b + 2v_0} \right) \right). \tag{187}$$

This leads to, for $x < 0$, using (169)

$$1 + 2r(x) = -\frac{2v_0 + b}{b} W \left(-\frac{2b}{2a + b + 2v_0} e^{A_- x - \frac{2b}{2a + b + 2v_0}} \right), \quad A_- = \frac{8a\gamma}{(2v_0 + b)^2 - 4a^2}. \tag{188}$$

Taking the derivative we find the total density in phase II

$$\rho_s(x) = A_- \frac{2v_0 + b}{2b} \left(\frac{1}{1 + W \left(-\frac{2b}{2a + b + 2v_0} e^{A_- x - \frac{2b}{2a + b + 2v_0}} \right)} - 1 \right), \quad x < 0, \tag{189}$$

and we recall that $\rho_s(x) = 0$ for $x > 0$. The smooth part of the density reaches a finite limit $\rho_s(0^-) = (b + 2v_0)A_-/(2a - b + 2v_0)$ at $x = 0^-$. Furthermore, there is a delta peak at $x = 0$ (which contains only + particles) with weight

$$\frac{1}{2} - r(0^-) = \frac{2a}{b + 2v_0 + 2a}. \tag{190}$$

3. Phase III: Shock at $x = 0$

We now turn to the last region, where $b/2 > v_0 + a$. This corresponds to the regime where the repulsion exerted by the $+$ particles on the $-$ particles is strong enough to allow the $-$ particles to access the region $x > 0$. Indeed in this regime, our numerical simulations show the presence of a cluster of $+$ particles at $x = 0$ and a non-zero density on the whole real axis. This suggests that the $+$ particles remain stuck at $x = 0$ while the $-$ particles located at $x = 0$ can go either to the left or to the right depending on the fluctuations. The absence of $-$ particles in the cluster suggests to impose the continuity of $h_-(x)$ at 0, i.e. $h_-(0^-) = h_-(0^+) = h_-(0)$. The computation of the two integration constants requires an additional boundary condition. This can be obtained by considering the forces near $x = 0$. The fact that $-$ particles are able to go either to the right or to the left requires $f_-(0^+) > 0$ and $f_-(0^-) < 0$, but also that the force exactly at $x = 0$ vanishes

$$f_-(0) = -v_0 + b(h_+(0^+) + h_+(0^-)) = 0. \quad (191)$$

Rewriting (160), in terms of $h_{\pm}(x)$, we have

$$h_+(0^+) - h_-(0^+) = \frac{a}{b - 2v_0}(1 - 2(h_+(0^+) + h_-(0^+))), \quad (192)$$

$$h_+(0^-) - h_-(0^-) = -\frac{a}{b + 2v_0}(1 + 2(h_+(0^-) + h_-(0^-))), \quad (193)$$

which can be rewritten as

$$h_+(0^+) = h_-(0^+) + \frac{a}{2a + b - 2v_0}(1 - 4h_-(0^+)), \quad (194)$$

$$h_+(0^-) = h_-(0^-) - \frac{a}{2a + b + 2v_0}(1 + 4h_-(0^-)). \quad (195)$$

Using the continuity of $h_-(x)$ and the condition (191), we obtain

$$\begin{aligned} h_-(0) &= \frac{v_0 b^2 + 4a^2 - 4v_0^2}{2b b^2 - 4a^2 - 4v_0^2}, \\ h_+(0^+) &= \frac{\frac{4a^2(b-2a)}{4a^2-b^2+4v_0^2} + 2a + v_0}{2b}, \\ h_+(0^-) &= \frac{\frac{4a^2(2a-b)}{4a^2-b^2+4v_0^2} - 2a + v_0}{2b}. \end{aligned} \quad (196)$$

Note that $h_-(0) > 0$ so that there are more $-$ particles (and thus also more $+$ particles) on the left than on the right. One can check that on the line $b/2 = v_0 + a$ one has $h_-(0) = 1/4$ and $h_+(0^+) = 1/4$. In addition, one can check that

$$f_+(0^+) = v_0 - a - 2bh_-(0) < 0, \quad f_+(0^-) = v_0 + a - 2bh_-(0) > 0, \quad (197)$$

$$f_-(0^+) = -v_0 - a + 2bh_+(0^+) > 0, \quad f_-(0^-) = -v_0 + a + 2bh_+(0^-) < 0, \quad (198)$$

which validates our assumptions.

Eq. (196) leads to

$$1 - 2r(0^+) = \frac{(b^2 - 4v_0^2)(b - 2a - 2v_0)}{b(b^2 - 4a^2 - 4v_0^2)}, \quad (199)$$

$$1 + 2r(0^-) = \frac{(b^2 - 4v_0^2)(b - 2a + 2v_0)}{b(b^2 - 4a^2 - 4v_0^2)}, \quad (200)$$

which, inserting into (163) and (168) for $x = 0$ gives

$$C_+ = \frac{(b^2 - 4v_0^2)(b - 2a - 2v_0)}{b^2 - 4a^2 - 4v_0^2} + (2v_0 - b) \log \left(\frac{(b^2 - 4v_0^2)(b - 2a - 2v_0)}{b(b^2 - 4a^2 - 4v_0^2)} \right), \quad (201)$$

$$C_- = \frac{(b^2 - 4v_0^2)(b - 2a + 2v_0)}{b^2 - 4a^2 - 4v_0^2} - (b + 2v_0) \log \left(\frac{(b^2 - 4v_0^2)(b - 2a + 2v_0)}{b(b^2 - 4a^2 - 4v_0^2)} \right). \quad (202)$$

This leads to the solution, for $a < -v_0 + b/2$,

$$1 - 2r(x) = \frac{2v_0 - b}{b} W(-B_+ e^{-A_+ x - B_+}), \quad A_+ = \frac{8a\gamma}{(2v_0 - b)^2 - 4a^2}, \quad B_+ = \frac{(b + 2v_0)(b - 2a - 2v_0)}{b^2 - 4a^2 - 4v_0^2}, \quad (203)$$

$$1 + 2r(x) = -\frac{2v_0 + b}{b} W(-B_- e^{A_- x - B_-}), \quad A_- = \frac{8a\gamma}{(2v_0 + b)^2 - 4a^2}, \quad B_- = \frac{(b - 2v_0)(b - 2a + 2v_0)}{b^2 - 4a^2 - 4v_0^2}, \quad (204)$$

Finally, the total density in phase III reads

$$\rho_s(x) = A_+ \frac{b - 2v_0}{2b} \left(\frac{1}{1 + W(-B_+ e^{-A_+ x - B_+})} - 1 \right), \quad x > 0, \quad (205)$$

$$\rho_s(x) = A_- \frac{2v_0 + b}{2b} \left(\frac{1}{1 + W(-B_- e^{A_- x - B_-})} - 1 \right), \quad x < 0, \quad (206)$$

with a delta peak at $x = 0$ with weight

$$h_+(0^+) - h_+(0^-) = \frac{2a(b^2 - 2ab - 4v_0^2)}{b(b^2 - 4a^2 - 4v_0^2)}. \quad (207)$$

We compared our analytical results to numerical simulations for finite N in Fig. 4 (see Sec. II for a discussion). Note that in phase III case, the convergence with N is slower than in the other regimes (see Fig. 4) due to the particular role played by the fluctuations.

V. CONCLUSION

In this paper, we studied two different models of run-and-tumble particles with 1D Coulomb interaction: the active jellium model, with a harmonic external potential, and the non-reciprocal active self-gravitating gas, with a non-reciprocal rank interaction and a linear confining potential. Both models converge at large time to a steady state which exhibits a number of phase transitions. In both cases, we achieved significant analytical progress in the computation of the stationary particle density in the large N limit, allowing for a thorough understanding of the different phases of the two models.

Concerning the non-reciprocal self-gravitating gas, there is a lot of space left for extensions of the model. First, one could consider different confining potentials or study the large time behavior in the absence of confinement. Second one could try to generalize the present computation by adding a reciprocal part to the interaction on top of the non-reciprocal component. This would allow to test whether the shocks which occur at the edge for purely a reciprocal rank interaction [68] are modified in this case. Finally, it would be interesting to extend the present model to a case where the non-reciprocal interaction takes place between two distinct species of particles, independently of their velocity state. Of course, we expect the behavior to be very different in this case. More generally, despite their relevance for biological systems, few exact results have been obtained until now for models of active particles with non-reciprocal interactions. We hope that the present paper will provide tools for more analytical studies of such models in the future.

Acknowledgments. We acknowledge support from ANR Grant No. ANR- 23-CE30-0020-01 EDIPS.

Appendix A: "Vision cone" model

Let us consider another non-reciprocal extension of the active rank diffusion model, inspired from models with "vision cones". Each particle now only receives a force only from the particles which are in front of it (i.e. on the right for + particles and on the left for - particles). The equations of motion read,

$$\dot{x}_i = -\sigma_i(t) \frac{2\kappa}{N} \sum_{j \neq i} \Theta(\sigma_i(t)(x_j - x_i)) - V'(x_i) + v_0 \sigma_i(t), \quad (\text{A1})$$

where $\Theta(x)$ is the Heaviside function and we choose the convention $\Theta(0) = 1/2$. Writing $\Theta(x) = \frac{1}{2}(1 + \text{sgn}(x))$, this can be rewritten as (up to a term $\sigma_i \kappa / N$ which we neglect)

$$\dot{x}_i = \sigma_i(t) \left[v_0 - \kappa - \frac{\kappa}{N} \sum_{j \neq i} \text{sgn}(\sigma_i(t)(x_j - x_i)) \right] - V'(x_i) \quad (\text{A2})$$

$$= \sigma_i(t) (v_0 - \kappa) - \frac{\kappa}{N} \sum_{j \neq i} \text{sgn}(x_j - x_i) - V'(x_i). \quad (\text{A3})$$

Quite surprisingly, this is exactly the same equation as the reciprocal active rank diffusion model (1) with a mapping $v_0 \rightarrow \tilde{v}_0 = v_0 - \kappa$. The non-reciprocity does not play any particular role in this case and the phase diagram can be directly deduced from the one that we have obtained in the reciprocal case, in [68] for $V(x) = 0$ and $V(x) = a|x|$, and in the present paper for $V(x) = \frac{\mu}{2}x^2$. Note however that here the effective driving velocity \tilde{v}_0 may be negative, but changing the sign of the velocity simply amounts to exchanging + and - particles so that the full phase diagrams can be obtained by symmetry. This exchange of + and - particles only occurs in the repulsive case $\kappa > 0$ and is due to the fact that a - particle located far at the right will "see" the other particles and be repulsed towards the right, while a + particle will feel no interaction (and vice-versa at the left edge). More precisely, the phase diagrams remain the same up to a replacement of v_0 by $|\tilde{v}_0|$ (we only need to recall that + and - particles are exchanged whenever $\tilde{v}_0 < 0$). Some regions of the phase diagram will however become inaccessible. In the repulsive case, one has $\tilde{v}_0/\kappa = v_0/\kappa - 1 \in [-1, \infty)$ (or $\kappa/\tilde{v}_0 = \frac{1}{v_0/\kappa - 1} \in (-\infty, -1) \cup (0, \infty)$), thus the entire diagram is still accessible. But in the attractive case, $\tilde{v}_0/\bar{\kappa} = v_0/\bar{\kappa} + 1 \in [1, \infty)$ (or $\bar{\kappa}/\tilde{v}_0 = \frac{1}{v_0/\bar{\kappa} + 1} \in (0, 1)$), which means that some regions of the diagram do not exist in this model. In particular, in the absence of external potential, in the attractive case it implies that the density is always smooth, with unbounded support (i.e. the phase I_s in [68]) and there is no transition (in the repulsive case, the solution is again an expanding plateau, with support $[-\kappa t, \kappa t]$). In the case of a linear or harmonic confinement however, all the different phases continue to exist, although for some of them in a reduced domain.

-
- [1] P. Hänggi and P. Jung, *Colored Noise in Dynamical Systems*, Adv. Chem. Phys. **89**, 239 (1995).
 - [2] G. H. Weiss, *Some applications of persistent random walks and the telegrapher's equation*, Physica A **311**, 381 (2002).
 - [3] J. Masoliver and K. Lindenberg, *Continuous time persistent random walk: a review and some generalizations*, Eur. Phys. J. B **90**, 1 (2017).
 - [4] M. Kac, *A stochastic model related to the telegrapher's equation*, Rocky Mountain J. Math. **4**, 497 (1974).
 - [5] E. Orsingher, *Probability law, flow function, maximum distribution of wave-governed random motions and their connections with Kirchoff's laws*, Stoch. Process. Their Appl. **34**, 49 (1990).
 - [6] H. C. Berg, *E. Coli in Motion*, (Springer Verlag, Heidelberg, Germany) (2004).
 - [7] J. Tailleur, and M. E. Cates, *Statistical mechanics of interacting run-and-tumble bacteria*, Phys. Rev. Lett. **100**, 218103 (2008).
 - [8] D. Boriskovsky, D. Cohen, *Negative mobility, sliding and delocalization for stochastic networks*, Phys. Rev. E **101**, 062129 (2020).
 - [9] D. Shapira, D. Cohen, *Emergence of Sinai Physics in the stochastic motion of passive and active particles*, New J. Phys. **24**, 063026 (2022).

- [10] A. P. Solon, Y. Fily, A. Baskaran, M. E. Cates, Y. Kafri, M. Kardar, and J. Tailleur, *Pressure is not a state function for generic active fluids*, Nature Phys. **11**, 673 (2015).
- [11] S. C. Takatori, R. De Dier, J. Vermant, and J. F. Brady, *Acoustic trapping of active matter*, Nature Comm. **7**, 10694 (2016).
- [12] A. Dhar, A. Kundu, S. N. Majumdar, S. Sabhapandit and G. Schehr, *Run-and-tumble particle in one-dimensional confining potentials: Steady-state, relaxation, and first-passage properties*, Phys. Rev. E **99**, 032132 (2019).
- [13] O. Dauchot and V. Démery, *Dynamics of a Self-Propelled Particle in a Harmonic Trap*, Phys. Rev. Lett. **122**, 068002 (2019).
- [14] U. Basu, S. N. Majumdar, A. Rosso, S. Sabhapandit, and G. Schehr, *Exact stationary state of a run-and-tumble particle with three internal states in a harmonic trap*, J. Phys. A: Math. Theor. **53**, 09LT01 (2020)
- [15] P. Le Doussal, S. N. Majumdar, and G. Schehr, *Velocity and diffusion constant of an active particle in a one-dimensional force field*, EPL **130**, 40002 (2020).
- [16] M. C. Marchetti, J. F. Joanny, S. Ramaswamy, T. B. Liverpool, J. Prost, M. Rao, and R. Aditi Simha, *Hydrodynamics of soft active matter*, Rev. Mod. Phys. **85**, 1143 (2013).
- [17] C. Bechinger, R. Di Leonardo, H. Löwen, C. Reichhardt, G. Volpe, and G. Volpe, *Active particles in complex and crowded environments*, Rev. Mod. Phys. **88**, 045006 (2016).
- [18] S. Ramaswamy, *Active Matter*, J. Stat. Mech. 054002, (2017).
- [19] É. Fodor, and M. C. Marchetti, *The statistical physics of active matter: from self-catalytic colloids to living cells*, Physica A **504**, 106 (2018).
- [20] M. E. Cates, *Diffusive transport without detailed balance: Does microbiology need statistical physics ?*, Rep. Prog. Phys. **75**, 042601 (2012).
- [21] Y. Fily, and M. C. Marchetti, *Athermal phase separation of self-propelled particles with no alignment*, Phys. Rev. Lett. **108**, 235702 (2012).
- [22] I. Buttinoni, J. Bialké, F. Kummel, H. Lowen, C. Bechinger, and T. Speck, *Dynamical Clustering and Phase Separation in Suspensions of Self-Propelled Colloidal Particles*, Phys. Rev. Lett. **110**, 238301 (2013).
- [23] Y. Fily, S. Henkes, and M. C. Marchetti, *Freezing and phase separation of self-propelled disks*, Soft matter **10**, 2132 (2014).
- [24] M. Cates, and J. Tailleur, *Motility-induced phase separation*, Annu. Rev. Condens. Matter Phys. **6**, 219 (2015).
- [25] A. B. Slowman, M. R. Evans, and R. A. Blythe, *Jamming and attraction of interacting run-and-tumble random walkers*, Phys. Rev. Lett. **116**, 218101 (2016).
- [26] A. B. Slowman, M. R. Evans, and R. A. Blythe, *Exact solution of two interacting run-and-tumble random walkers with finite tumble duration*, J. Phys. A: Math. Theor. **50**, 375601 (2017).
- [27] D. Martin, J. O’Byrne, M. E. Cates, E. Fodor, C. Nardini, J. Tailleur, F. van Wijland, *Statistical mechanics of active Ornstein-Uhlenbeck particles*, Phys. Rev. E **103**, 032607 (2021).
- [28] C. M. Barriuso Gutiérrez, C. Vanhille-Campos, Francisco Alarcon, I. Pagonabarraga, R. Britoai, and C. Valeriani, *Collective motion of run-and-tumble repulsive and attractive particles in one-dimensional systems*, Soft Matter **17**(46) (2021).
- [29] M. E. Cates, D. Marenduzzo, I. Pagonabarraga, and J. Tailleur, *Arrested phase separation in reproducing bacteria creates a generic route to pattern formation*, Proc. Natl. Acad. Sci. U.S.A. **107**, 11715 (2010).
- [30] R. Soto, R. Golestanian, *Run-and-tumble dynamics in a crowded environment: Persistent exclusion process for swimmers*, Phys. Review E **89**, 012706 (2014).
- [31] M. Kourbane-Houssene, C. Erignoux, T. Bodineau, and J. Tailleur, *Exact Hydrodynamic Description of Active Lattice Gases*, Phys. Rev. Lett. **120**, 268003 (2018).
- [32] T. Agranov, S. Ro, Y. Kafri, and V. Lecomte, *Exact fluctuating hydrodynamics of active lattice gases-typical fluctuations*, J. Stat. Mech. 083208 (2021).
- [33] T. Agranov, S. Ro, Y. Kafri, and V. Lecomte, *Macroscopic Fluctuation Theory and Current Fluctuations in Active Lattice Gases*, [arXiv:2208.02124](https://arxiv.org/abs/2208.02124).
- [34] P. Le Doussal, S. N. Majumdar, G. Schehr, *Stationary nonequilibrium bound state of a pair of run and tumble particles*, Physical Review E **104**(4), 044103 (2021).
- [35] P. Dolai, S. Krekels, and C. Maes, *Inducing a bound state between active particles*, [arXiv:2202.04459](https://arxiv.org/abs/2202.04459) (2022).
- [36] I. Mukherjee, A. Raghu, and P. K. Mohanty, *Nonexistence of motility induced phase separation transition in one dimension*, [arXiv:2208.05937](https://arxiv.org/abs/2208.05937).
- [37] E. Mallmin, R. A. Blythe, and M. R. Evans, *Exact spectral solution of two interacting run-and-tumble particles on a ring lattice*, J. Stat. Mech., 013204 (2019).
- [38] A. Das, A. Dhar, and A. Kundu, *Gap statistics of two interacting run and tumble particles in one dimension*, J. Phys. A: Math. Theor. **53**, 345003 (2020).
- [39] P. Le Doussal, S. N. Majumdar, and G. Schehr, *Noncrossing run-and-tumble particles on a line*, Phys. Rev. E **100**, 012113 (2019).

- [40] P. Singh, A. Kundu, *Crossover behaviours exhibited by fluctuations and correlations in a chain of active particles*, J. Phys. A: Math. Theor. **54**, 305001 (2021)
- [41] S. Put, J. Berx, and C. Vanderzande, *Non-Gaussian anomalous dynamics in systems of interacting run-and-tumble particles*, J. Stat. Mech. 123205 (2019).
- [42] S. Prakash, U. Basu, S. Sabhapandit, *Tagged particle behavior in a harmonic chain of direction reversing active Brownian particles*, J. Stat. Mech. (2024) 083211.
- [43] S. Paul, A. Dhar, D. Chaudhuri, *Dynamical crossovers and correlations in a harmonic chain of active particles*, Soft Matter (2024).
- [44] M. J. Metson, M. R. Evans, and R. A. Blythe, *Tuning attraction and repulsion between active particles through persistence*, EPL **141**, 41001 (2023).
- [45] M. J. Metson, M. R. Evans, and R. A. Blythe, *From a microscopic solution to a continuum description of interacting active particles*, Phys. Rev. E **107**, 044134 (2023).
- [46] R. Dandekar, S. Chakraborti, and R. Rajesh, *Hard core run and tumble particles on a one-dimensional lattice*, Phys. Rev. E **102**, 062111 (2020).
- [47] A. G. Thompson, J. Tailleur, M. E. Cates, R. A. Blythe, *Lattice models of nonequilibrium bacterial dynamics*, J. Stat. Mech. P02029 (2011).
- [48] L. Touzo, P. Le Doussal, G. Schehr, *Interacting, running and tumbling: the active Dyson Brownian motion*, EPL **142**, 61004 (2023) or [arXiv:2302.02937](https://arxiv.org/abs/2302.02937).
- [49] For RD see Section 5.5, and for more general models where the stationary measure has a product form see e.g. Corollary 4.8 in N. O'Connell, J. Ortmann, *Product-form invariant measures for Brownian motion with drift satisfying a skew-symmetry type condition*, ALEA, Lat. Am. J. Probab. Math. Stat. **11**, 307 (2014).
- [50] S. Pal, J. Pitman, *One-dimensional Brownian particle systems with rank-dependent drifts*, Ann. Appl. Probab. **18**, 2179 (2008).
- [51] A. D. Banner, R. Fernholz, I. Karatzas, *Atlas models of equity markets*, Ann. Appl. Probab. **15**, 2296 (2005)
- [52] G. B. Rybicki, *Exact statistical mechanics of a one-dimensional self-gravitating system*, Astrophys. Space Sci. **14**, 56 (1971).
- [53] P. H. Chavanis, C. Sire, *Anomalous diffusion and collapse of self-gravitating Langevin particles in D dimensions*, Phys. Rev. E **69**, 016116 (2004).
- [54] P. Kumar, B. N. Miller, D. Pirjol, *Thermodynamics of a one-dimensional self-gravitating gas with periodic boundary conditions*, Phys. Rev. E **95**, 022116 (2017).
- [55] A. Lenard, *Exact statistical mechanics of a one-dimensional system with Coulomb forces*, J. Math. Phys. **2**, 682 (1961).
- [56] S. Prager, *The One-Dimensional Plasma*, Adv. Chem. Phys. **4**, 201 (1962).
- [57] R. J. Baxter, *Statistical mechanics of a one-dimensional Coulomb system with a uniform charge background*, Proc. Camb. Phil. Soc. **59**, 779 (1963)
- [58] D. S. Dean, R. R. Horgan, A. Naji, R. Podgornik, *Effects of dielectric disorder on van der Waals interactions in slab geometries*, Phys. Rev. E **81**, 051117 (2010)
- [59] G. Tellez, E. Trizac, *Screening like charges in one-dimensional Coulomb systems: Exact results*, Phys. Rev. E **92**, 042134 (2015).
- [60] For a recent review, see M. Lewin, *Coulomb and Riesz gases: The known and the unknown*, J. Math. Phys. **63**, 061101 (2022).
- [61] A. Dhar, A. Kundu, S. N. Majumdar, S. Sabhapandit, G. Schehr, *Exact extremal statistics in the classical 1d Coulomb gas*, Phys. Rev. Lett. **119**, 060601 (2017).
- [62] A. Dhar, A. Kundu, S. N. Majumdar, S. Sabhapandit, G. Schehr, *Extreme statistics and index distribution in the classical 1d Coulomb gas*, J. Phys. A: Math. and Theor., **51**, 295001 (2018).
- [63] A. Flack, S. N. Majumdar, G. Schehr, *Truncated linear statistics in the one dimensional one-component plasma*, J. Phys. A: Math. Theor. **54**, 435002 (2021).
- [64] A. Flack, S. N. Majumdar, G. Schehr, *Gap probability and full counting statistics in the one-dimensional one-component plasma*, J. Stat. Mech. 053211 (2022).
- [65] D. Chafai, D. Garcia-Zelada, P. Jung, *At the edge of a one-dimensional jellium*, Bernoulli **28**, 1784 (2022).
- [66] P. Le Doussal, *Ranked diffusion, delta Bose gas and Burgers equation*, Phys. Rev. E **105**, L012103 (2022).
- [67] A. Flack, P. Le Doussal, S. N. Majumdar, G. Schehr, *Out of equilibrium dynamics of repulsive ranked diffusions: the expanding crystal*, Phys. Rev. E **107**, 064105 (2023).
- [68] L. Touzo and P. Le Doussal, *Non-equilibrium phase transition in active rank diffusions*, EPL **145**, 41001 (2024) or [arXiv:2308.06118](https://arxiv.org/abs/2308.06118).
- [69] M. Fruchart, R. Hanai, P. B. Littlewood, V. Vitelli, *Non-reciprocal phase transitions*, Nature **592**(7854), 363-369 (2021).
- [70] A. Haluts, D. Gorbonos, N.S. Gov, *Models of Animal Behavior as Active Particle Systems with Nonreciprocal Interactions*, in J.A. Carrillo, E. Tadmor, (eds) Active Particles, Volume 4: Modeling and Simulation in Science,

- Engineering and Technology, Springer Nature Switzerland, Birkhäuser, Cham (2024).
- [71] A. Kocabas, S. Ozdemir, M. Basaran, T. Yüce, A. Kecebas, B. Altin, Y. Yaman, E. Demir, C. Kocabas, *Non-reciprocal phase transition enables swarming motility in biological active matter*, preprint available at Research Square [https://doi.org/10.21203/rs.3.rs-3956047/v1] (2024).
 - [72] N. S. Mandal, A. Sen, R. D. Astumian, *A molecular origin of non-reciprocal interactions between interacting active catalysts*, Chem. **10** (4), 1147-1159 (2024).
 - [73] Z. You, A. Baskaran, M. C. Marchetti, *Nonreciprocity as a generic route to traveling states*, Proc. Natl. Acad. Sci. U.S.A. **117** (33) 19767-19772 (2020).
 - [74] D. Martin, D. Seara, Y. Avni, M. Fruchart, V. Vitelli, *The transition to collective motion in nonreciprocal active matter: coarse graining agent-based models into fluctuating hydrodynamics*, arXiv:2307.08251 (2023).
 - [75] K. L. Kreienkamp, S. H. L. Klapp, *Clustering and flocking of repulsive chiral active particles with non-reciprocal couplings*, New J. Phys. **24**, 123009 (2022).
 - [76] M. Knezevic, T. Welker, H. Stark, *Collective motion of active particles exhibiting non-reciprocal orientational interactions*, Sci. Rep. **12**, 19437 (2022).
 - [77] A. Dinelli, J. O'Byrne, A. Curatolo, Y. Zhao, P. Sollich, J. Tailleur, *Non-reciprocity across scales in active mixtures*, Nat. Commun. **14**, 7035 (2023).
 - [78] Y. Duan, J. Agudo-Canalejo, R. Golestanian, B. Mahault, *Dynamical Pattern Formation without Self-Attraction in Quorum-Sensing Active Matter: The Interplay between Nonreciprocity and Motility*, Phys. Rev. Lett. **131**, 148301 (2023).
 - [79] Y. Duan, J. Agudo-Canalejo, R. Golestanian, B. Mahault, *Phase Coexistence in Nonreciprocal Quorum-Sensing Active Matter*, arXiv:2411.05465 (2024).
 - [80] M. Du, S. Vaikuntanathan, *Hidden nonreciprocity as a stabilizing effective potential in active matter*, arXiv:2401.14690 (2024).
 - [81] J. P. Newman, H. Sayama, *Effect of sensory blind zones on milling behavior in a dynamic self-propelled particle model*, Phys. Rev. E **78**, 011913 (2008).
 - [82] L. Barberis, F. Peruani, *Large-Scale Patterns in a Minimal Cognitive Flocking Model: Incidental Leaders, Nematic Patterns, and Aggregates*, Phys. Rev. Lett. **117**, 248001 (2016).
 - [83] F. Peruani, *Hydrodynamic Equations for Flocking Models without Velocity Alignment*, J. Phys. Soc. Jpn. **86**, 101010 (2017).
 - [84] M. Durve, A. Saha, A. Sayeed, *Active particle condensation by non-reciprocal and time-delayed interactions*, Eur. Phys. J. E **41**, 49 (2018).
 - [85] R. Singh Negi, R. G. Winkler, G. Gompper, *Emergent collective behavior of active Brownian particles with visual perception*, Soft Matter **18**, 6167 (2022).
 - [86] J. Qi, L. Bai, Y. Xiao, Y. Wei, W. Wu, *The emergence of collective obstacle avoidance based on a visual perception mechanism*, Information Sciences **582**, 850-864 (2022).
 - [87] P. Stengele, A. Lüders, P. Nielaba, *Group formation and collective motion of colloidal rods with an activity triggered by visual perception*, Phys. Rev. E **106** (2022).
 - [88] R. Saavedra1, F. Peruani, *Self-trapping of active particles with non-reciprocal interactions in disordered media*, arXiv:2404.10932 (2024).
 - [89] D. S. Dean, *Langevin Equation for the density of a system of interacting Langevin processes*, J. Phys. A: Math. Gen. **29**, L613 (1996).
 - [90] K. Kawasaki, *Microscopic analyses of the dynamical density functional equation of dense fluids*, J. Stat. Phys. **93**, 527 (1998).